A fractional viscoelastic model for laminated glass sandwich plates under blast actions

A fractional viscoelastic model for laminated glass sandwich plates under blast actions

Luca Viviani[1 4], Mario Di Paola[2], and Gianni Royer-Carfagni[*1 3]

[1]Department of Engineering and Architecture, University of Parma, Parco Area delle Scienze 181/A, I-43100 Parma, Italy
[2]Department of Engineering, University of Palermo Viale delle Scienze, I 90128 Palermo, Italy
[3]Construction Technologies Institute - Italian National Research Council (ITC-CNR), Via Lombardia 49, I-20098 San Giuliano Milanese, Milano, Italy
[4]Maffeis Engineering SpA, Via Mignano 26, I-36020 Solagna, Vicenza, Italy

Abstract

A model is proposed to evaluate the effects of explosions on laminated glass plates, made of glass plies bonded by thin polymeric interlayers, in the pre-glass-breakage phase. The novelty consists in the description of the viscoelastic properties of the interlayer, based on fractional calculus. This has noteworthy advantages because the relaxation function of most commercial polymers can be well approximated by power laws in the time interval of interest: in the fractional approach, this trend can be directly described by only two material parameters, whereas the traditional Prony series requires many more coefficients to be calibrated. Modelling of the plate is layerwise and the coupling with an elastic supporting back structure is considered. The glass plies are Kirchhoff-Love plates, whereas the impinging pressure from the explosion follows Friedlander equation. The governing equations, found via Hamilton's principle, are solved à la Galerkin through a spatial expansion in Fourier series

[*]Corresponding author
Email addresses: gianni.royer@unipr.it (Gianni Royer-Carfagni), mario.dipaola@unipa.it (Mario Di Paola), luca.viviani@unipr.it (Luca Viviani)

and a step-by-step integration in time using the Grünwald-Letnikov operators. Numerical experiments aim at describing how the fractional parameters of the interlayer, as well the compliance/mass of the back structure, affect the stress and deflection of the laminated plate. Comparisons are made with the commonly used quasi-elastic approximation, which considers the interlayer as linear elastic. The results show that the viscosity of the interlayer cannot in general be neglected and how a compliant back structure can help to safeguard the glass, although its displacement may exceed the serviceability limits. The optimal design shall thus represent a compromise between different effects: despite its limitation, the proposed model can represent a tool to make a correct choice.

Keywords: Sandwich plates; laminated glass; viscoelasticity; fractional calculus; explosive shocks; dynamics.

Contents

1 Introduction

Laminated glass is a composite formed by two (or more) glass plies sandwiching one (or more) polymeric foil(s), permanently bonded with a process at high temperature

and pressure in autoclave. The polymeric interlayer is too thin to present bending capacity, but it contributes to the stiffness and strength of the laminate by shear coupling the glass plies. Moreover, the interlayer prevents the detachment of potentially injuring fragments in the post-breakage phase [1–3]. Laminated glass is commonly used to manufacture large transparent windows in prestigious buildings, but one of the most challenging applications is certainly that of bomb-blast resistant façades, an issue related to the threat of terroristic events. The purpose of this work is twofold: firstly, a structural model for laminated glass plates in the pre-glass-breakage stage is introduced, where fractional calculus is used to describe the viscoelastic constitutive behaviour of the interlayer; secondly, numerical experiments are carried out in order to highlight how the viscoelastic contribution affects the dynamic response of a simply supported plate under blast loads.

The most common approach to reproduce the viscoelasticity of commercial polymeric interlayers relies upon the Wiechert rheological scheme of spring/dashpot Maxwell units assembled in parallel [4–6]. The relaxation of each unit is an exponential function, which forms a reverse "s"-like shaped curve in the bi-logarithmic stress-time chart. The assembly of various units produces a sum of exponentials commonly referred to as *Prony series*, which usually requires more than 15-20 terms to reach an acceptable precision in the service time scale. However, for load durations of the order of some milliseconds, as in the case of explosions, the relaxation function of most polymers can be well interpreted by a power law [7–9], which is a straight line in the bi-logarithmic stress-time plane. This observation strongly recommends the use of a *fractional* viscoelastic constitutive model, in which the time dependence is expressed via fractional differentiation of order α, with $0 < \alpha < 1$. Viscoelastic models of this kind have been proposed in the technical literature [10–12]: consistency with thermodynamic principles and realistic predictions are in favor of this approach [13–15]. It is important to remark that, whereas a number of parameters would be necessary to fit a power law with a Prony series, only two parameters enter into the fractional viscoelastic constitutive equation. The calibration from experiments is thus facilitated, and the mathematical description of the structural response more straightforward [16–21].

The effects of the explosion on the plate are modelled as a uniformly distributed pressure that varies in time according to Friedlander wave form [22,23]. This is a short

duration (impulsive) action, composed of an initial pressure peak that exponentially decays, forming a subsequent suction phase (negative pressure). The parameters of such action have been derived from Standards, which provide specific rules to design glass components in explosive scenarios, in the form of empirical relations and experimental procedures to asses the pre-/post-breakage phases [24–28]. Our interest here is for the pre-glass-breakage phase only, which assumes that the glass plies remain sound under the blast loading event.

Three-layer laminated glass beams (1-D model) were studied [29, 30] by considering, from a theoretical point of view, just a few terms in the Prony series to define the viscoelastic response of the interlayer. The same structural scheme has been recently extended to a fractional viscoelastic characterization [21]. However, the aforementioned studies consider only quasi-static actions, thus bypassing the solution of the full dynamic problem. Here, we consider a 2-D model for a square laminated glass plate, and we solve the dynamic problem under impinging pressures of very short duration, as resulting from an explosion. Linear elastic Kirchhoff-Love plate theory is used to model the glass plies, while the interlayer is supposed to be only subjected to shear stresses, which couple the glass layers at the price of a zig-zag warping of the laminate cross section. This is a layerwise approach, which outperforms the homogenized models based on the first-order [31] or higher-order [32] shear deformation theory.

It is important to remark that laminated glass represents a particular laminate, being characterized by thick and stiff glass plies, and very thin and compliant interlayers. This implies that the glass plies are mainly subject to bending stresses and the polymeric interlayers to shear stresses. At least as a first order approximation, it seems reasonable to consider a simplified kinematics, where the slip at the level of polymeric foil is the sole allowed shear deformation, while glass plies get deformed only by bending contribution [33]. Of course, more accurate structural models could be proposed for laminated glass, in particular accounting also for the effects of the membrane stress (Von Kármán plate theory) and the shear stress in the glass (Reissner-Mindlin plate theory). Kumar et al. conducted studies about multi-layer composites [34–38], showing how a high order zig-zag theory (parabolic shear stress variation across the thickness of each ply) can be efficiently applied to get results close

to the 3-D elasticity solution. Other works specifically addressed to laminated composites [39–44], explain how to reduce the number of kinematic variables by means of integral terms quantifying the shear deformation.

The equilibrium equations for a simply supported three-layer plate are here derived from Hamilton's principle and solved à la Galerkin, by expressing the kinematic variables in Fourier series over the spatial domain and integrating each term over the time with a step-by-step finite difference approach. The time history in terms of bending/shear stress and deflection is plotted for a three-layer panel of given size, laminated with interlayers with different properties. These may correspond to different-in-type materials, or to the same material in different environmental conditions [45], since an increase in the operating temperature makes the interlayer more compliant, and vice versa. Considerations are made regarding how to deduce from the experimental data the parameters that define the fractional viscoelastic behaviour, especially as regards the correct interpretation of the branches of the relaxation function that can be defined with a power law.

Numerical experiments demonstrate how the viscoelasticity at the level of the interlayer affects the dynamic response of a laminated panel. This is comprised between the two borderline conditions [46] of *layered limit* (lower bound), with free-sliding glass plies, and *monolithic limit* (upper bound), where no sliding occurs between plies. The effect of a supporting back structure is considered by inserting an equivalent lumped mass oscillator in series with the laminated glass panel: a compliant back structure reduces the state of stress in the glass [47–49], but increases the displacement. Comparisons are also made with a simplified approach, usually referred to as the quasi elastic approximation [30], where the interlayer is supposed to be linear elastic, with a secant elastic modulus corresponding to the characteristic duration of the action. This simplification allows to capture well the first stress/deflection peak, but not the following ones because viscoelastic dissipation is neglected.

2 The fractional viscoelastic sandwich plate

The model problem is that of a sandwich plate, formed by two glass plies and one interposed polymeric foil. The governing equations and boundary conditions are

derived with a variational approach for a panel simply supported at the borders. The glass plies are Kirchhoff–Love plates, whereas a fractional viscoelastic constitutive model is used for the interlayer. The effect of the deformation of the load-bearing back structure is analytically modelled with a lumped mass connected in series with the plate by a spring-dashpot unit.

2.1 Governing equations for a simply supported plate

The schematic representation of the composite plate is that of Fig. 1(a). This is a three-layer plate composed by two thick elastic plies (layers "1" and "2") sandwiching one thin viscoelastic core (layer "0"). We introduce a reference frame with the (x, y) axes located in-plane, as indicated in the Figure, and z axis for each layer such that the mid-surface corresponds to $z = 0$. The external plies are Kirchhoff-Love plates; the core is too compliant to provide axial/bending stiffness, but it produces the shear coupling of the layers that are bonded through it, under the assumption that there is no sliding at the interfaces. The use of a Kirchhoff-Love linear plate theory is certainly a drastic approximation, which can be tolerated when the thickness of the plies is of the order of $1/50 - 1/100$ of the size of the plate.

The thickness of the external plies is denoted by h_i with $i = 1, 2$, so that the distance between the mid-planes reads

$$\bar{h} = h_0 + \frac{h_1 + h_2}{2}\,, \tag{2.1}$$

where h_0 represents the thickness of polymeric core. With reference to Figs. 1(b)-1(c), the interlayer "0" undergoes *shear strains*, which depend on the in-plane displacements $u_i = u_i(x, y, t)$ and $v_i = v_i(x, y, t)$ of the external layers, for $i = 1, 2$, as well as the out-of-plane displacement $w = w(x, y, t)$, which is the same for both layers. In particular, pure geometric considerations indicate that, within the hypothesis of infinitesimal deformations, the engineering shear strain components $\gamma_{x,0}$ and $\gamma_{y,0}$, considered independent of the variable z due to thinness of the interlayer, take the form

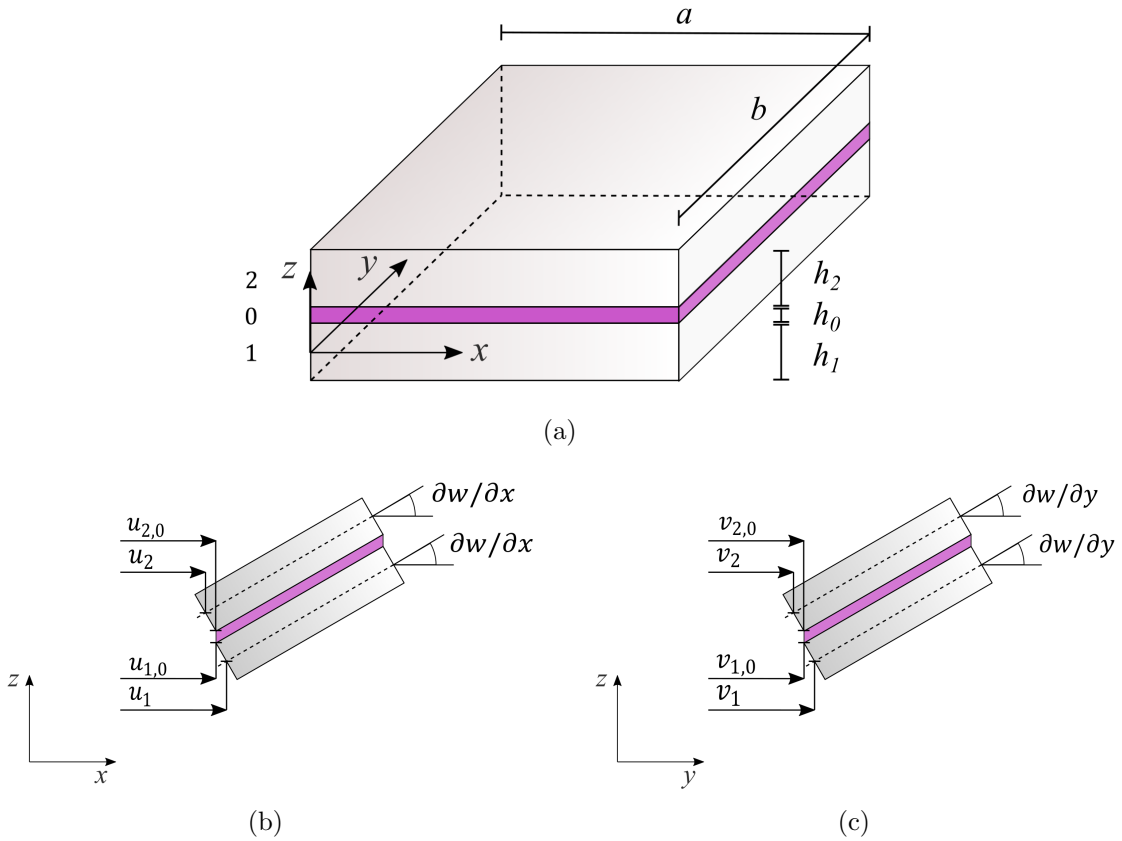

Figure 1: Schematic representation of a three-layered laminated glass plate. The glass plies are denoted as "1" and "2", while the core is the layer "0". For each layer, the reference system is located at one corner of the corresponding middle plane, with the z axis in the out-of-plane direction. The figure shows (a) the undistorted reference configuration and (b) the x-z view and the (c) y-z view of the deformed configuration of the plate, with indication of the variables used to describe the displacement.

$$\gamma_{x,0} = \gamma_{x,0}(x,y,t) = \frac{u_{2,0} - u_{1,0}}{h_0} + \frac{\partial w}{\partial x} = \frac{u_2 - u_1}{h_0} + \frac{\bar{h}}{h_0}\frac{\partial w}{\partial x}\,, \tag{2.2a}$$

$$\gamma_{y,0} = \gamma_{y,0}(x,y,t) = \frac{v_{2,0} - v_{1,0}}{h_0} + \frac{\partial w}{\partial y} = \frac{v_2 - v_1}{h_0} + \frac{\bar{h}}{h_0}\frac{\partial w}{\partial y}\,. \tag{2.2b}$$

For a constitutive model based on fractional calculus, recalled in the Appendix, the shear forces per unit length $Q_{x,0}$ and $Q_{y,0}$ depend on the shear stresses $\tau_{xz,0} = \tau_{xz,0}(x,y,t)$ and $\tau_{yz,0} = \tau_{yz,0}(x,y,t)$ reading

$$Q_{x,0} = Q_{x,0}(x,y,t) = \int_{-h_0/2}^{h_0/2} \tau_{xz,0}\, dz = C_\alpha\, {}^{C}_{0}\mathcal{D}^{\alpha}_{t}\left[u_2 - u_1 + \bar{h}\frac{\partial w}{\partial x}\right](t)\,, \tag{2.3a}$$

$$Q_{y,0} = Q_{y,0}(x,y,t) = \int_{-h_0/2}^{h_0/2} \tau_{yz,0}\, dz = C_\alpha\, {}^{C}_{0}\mathcal{D}^{\alpha}_{t}\left[v_2 - v_1 + \bar{h}\frac{\partial w}{\partial y}\right](t)\,, \tag{2.3b}$$

where C_α is a dimensional coefficient and α is the order of Caputo's fractional derivative (see Appendix A).

The strain components in the layers "1" and "2" ($\varepsilon_{x,i}$, $\varepsilon_{y,i}$, $\varepsilon_{xy,i}$, for $i = 1, 2$), are listed as follows

$$\varepsilon_{x,i} = \varepsilon_{x,i}(x,y,z,t) = \frac{\partial u_i}{\partial x} - z\frac{\partial^2 w}{\partial x^2}\,; \tag{2.4a}$$

$$\varepsilon_{y,i} = \varepsilon_{y,i}(x,y,z,t) = \frac{\partial v_i}{\partial y} - z\frac{\partial^2 w}{\partial y^2}\,; \tag{2.4b}$$

$$\varepsilon_{xy,i} = \varepsilon_{xy,i}(x,y,z,t) = \frac{\partial u_i}{\partial y} + \frac{\partial v_i}{\partial x} - 2z\frac{\partial^2 w}{\partial x \partial y}\,. \tag{2.4c}$$

The related stresses can be obtained from the corresponding constitutive relations. Denoting with E_i the Young's modulus and with ν_i the Poisson's ratio of the i^{th} layer, for $i = 1, 2$, the in-plane forces per unit length can be written as

$$N_{x,i} = N_{x,i}(x,y,t) = \int_{-h_i/2}^{h_i/2} \sigma_{x,i}\, dz = \frac{E_i h_i}{1-\nu_i^2}\left(\frac{\partial u_i}{\partial x} + \nu_i \frac{\partial v_i}{\partial y}\right), \tag{2.5a}$$

$$N_{y,i} = N_{y,i}(x,y,t) = \int_{-h_i/2}^{h_i/2} \sigma_{y,i}\, dz = \frac{E_i h_i}{1-\nu_i^2}\left(\frac{\partial v_i}{\partial y} + \nu_i \frac{\partial u_i}{\partial x}\right), \tag{2.5b}$$

$$N_{xy,i} = N_{xy,i}(x,y,t) = \int_{-h_i/2}^{h_i/2} \sigma_{xy,i}\, dz = \frac{E_i h_i}{2(1+\nu_i)}\left(\frac{\partial u_i}{\partial y} + \frac{\partial v_i}{\partial x}\right); \tag{2.5c}$$

while the bending moments per unit length are

$$M_{x,i} = M_{x,i}(x,y,t) = \int_{-h_i/2}^{h_i/2} \sigma_{x,i} z\, dz = -\frac{E_i h_i^3}{12(1-\nu_i^2)}\left(\frac{\partial^2 w}{\partial x^2} + \nu_i \frac{\partial^2 w}{\partial y^2}\right), \tag{2.6a}$$

$$M_{y,i} = M_{y,i}(x,y,t) = \int_{-h_i/2}^{h_i/2} \sigma_{x,i} z\, dz = -\frac{E_i h_i^3}{12(1-\nu_i^2)}\left(\frac{\partial^2 w}{\partial y^2} + \nu_i \frac{\partial^2 w}{\partial x^2}\right), \tag{2.6b}$$

$$M_{xy,i} = M_{xy,i}(x,y,t) = \int_{-h_i/2}^{h_i/2} \sigma_{xy,i} z\, dz = -\frac{E_i h_i^3}{12(1+\nu_i)}\left(\frac{\partial^2 w}{\partial x \partial y}\right). \tag{2.6c}$$

The governing equations can be deduced from Hamilton's principle, i.e.,

$$\int_{t_1}^{t_2} [\delta(\mathcal{K} - \mathcal{U}) + \delta\mathcal{W}_{\text{nc}} + \delta\mathcal{W}_{\text{ext}}]\, dt = 0\,, \tag{2.7}$$

where $\mathcal{K}$ represents the kinetic energy of the sandwich plate, $\mathcal{U}$ is the elastic energy, $\mathcal{W}_{\text{nc}}$ is the work made by the non-conservative forces and $\mathcal{W}_{\text{ext}}$ is the work of the external load.

By neglecting the kinetic energy associated to in-plane trajectories, one finds

$$\mathcal{K} = \frac{1}{2}\mu \int_A \dot{w}^2\, dA\,, \tag{2.8}$$

where $\mu = \rho_0 h_0 + \rho_1 h_1 + \rho_2 h_2$ is global mass per unit area, having denoted with ρ_j, $j = 0, 1, 2$ the densities of the corresponding layers.

The elastic energy presents two contributions, respectively related to the in-plane and bending deformations of the external plies only. Therefore, it reads

$$\mathcal{U} = \frac{1}{2}\int_A \sum_{i=1,2}\Bigg[N_{x,i}\frac{\partial u_i}{\partial x} + N_{y,i}\frac{\partial v_i}{\partial y} + N_{xy,i}\left(\frac{\partial u_i}{\partial y} + \frac{\partial v_i}{\partial x}\right) + M_{x,i}\frac{\partial^2 w}{\partial x^2} + M_{y,i}\frac{\partial^2 w}{\partial y^2} + 2M_{xy,i}\frac{\partial^2 w}{\partial x \partial y}\Bigg]\, dA\,. \tag{2.9}$$

The non-conservative work is due to the viscoelastic core, whose action is

$$\delta\mathcal{W}_{\rm nc} = \int_A \left[Q_{x,0}, \delta\gamma_{x,0} + Q_{y,0}\,\delta\gamma_{y,0}\right] dA\,. \tag{2.10}$$

Since the plate is loaded by a uniformly distributed force per unit area $p(t)$, the work performed by the external forces results

$$\delta\mathcal{W}_{\rm ext} = p\int_A \delta w\, dA\,. \tag{2.11}$$

In the considered case study, for simplicity both external plies are monoliths made of the same material (Young's modulus $E_1 = E_2 \equiv E_g$ and Poisson's ratio $\nu_1 = \nu_2 \equiv \nu$), and with the same thickness ($h_1 = h_2 \equiv h$). Their dimensions are thus indicated as $a \times b \times h$. Due to the geometric and load symmetry, $u_1 = -u_2$ and $v_1 = -v_2$. Hence, having defined $\Delta u = u_2 - u_1$ and $\Delta v = v_2 - v_1$, the problem is described by the three equilibrium equations

$$\begin{aligned}\mu\frac{\partial^2 w(x,y,t)}{\partial t^2} + \frac{E_g h^3}{6(1-\nu^2)}\left(\frac{\partial^4 w(x,y,t)}{\partial x^4} + 2\frac{\partial^4 w(x,y,t)}{\partial x^2\partial y^2} + \frac{\partial^4 w(x,y,t)}{\partial y^4}\right) \\ = \frac{\bar{h}}{h_0}C_\alpha\, {}_0^C\mathcal{D}_t^\alpha\left[\frac{\partial \Delta u(x,y,\cdot)}{\partial x} + \bar{h}\frac{\partial^2 w(x,y,\cdot)}{\partial x^2}\right](t) \\ + \frac{\bar{h}}{h_0}C_\alpha\, {}_0^C\mathcal{D}_t^\alpha\left[\frac{\partial \Delta v(x,y,\cdot)}{\partial y} + \bar{h}\frac{\partial^2 w(x,y,\cdot)}{\partial y^2}\right](t) + p(t)\,,\end{aligned} \tag{2.12a}$$

$$\frac{E_g h}{1-\nu^2}\left[\frac{\partial^2 \Delta u(x,y,t)}{\partial x^2}+\frac{1}{2}(1-\nu)\frac{\partial^2 \Delta u(x,y,t)}{\partial y^2}+\frac{1}{2}(1+\nu)\frac{\partial^2 \Delta v(x,y,t)}{\partial x \partial y}\right] = \frac{2}{h_0} C_\alpha \, {}_0^C\mathcal{D}_t^\alpha \left[\Delta u(x,y,\cdot)+\bar{h}\frac{\partial w(x,y,\cdot)}{\partial x}\right](t)\,, \quad (2.12b)$$

$$\frac{E_g h}{1-\nu^2}\left[\frac{\partial^2 \Delta v(x,y,t)}{\partial y^2}+\frac{1}{2}(1-\nu)\frac{\partial^2 \Delta v(x,y,t)}{\partial x^2}+\frac{1}{2}(1+\nu)\frac{\partial^2 \Delta u(x,y,t)}{\partial x \partial y}\right] = \frac{2}{h_0} C_\alpha \, {}_0^C\mathcal{D}_t^\alpha \left[\Delta v(x,y,\cdot)+\bar{h}\frac{\partial w(x,y,\cdot)}{\partial y}\right](t)\,. \quad (2.12c)$$

It is clear that the first equation represents the out-of-plane equilibrium, whereas the remaining two indicate the equilibrium in the x and y direction, respectively.

Hamilton's principle also provide the boundary conditions, which can synthetically stated in variational form as

$$\begin{aligned}
&-\int_{\partial\Omega}\sum_{i=1,2}\left[N_{x,i}n_x\delta u_i + N_{y,i}n_y\delta v_i + N_{xy,i}(n_y\delta u_i + n_x\delta v_i)\right]d\ell \\
&\quad -\int_{\partial\Omega}\sum_{i=1,2}\left[M_{x,i}n_x\frac{\partial\delta w}{\partial x}+M_{y,i}n_y\frac{\partial\delta w}{\partial y}+M_{xy}\left(n_y\frac{\partial\delta w}{\partial x}+n_x\frac{\partial\delta w}{\partial y}\right)\right]d\ell \\
&\quad +\int_{\partial\Omega}\sum_{i=1,2}\left[\frac{\partial M_{x,i}}{\partial x}n_x+\frac{\partial M_{y,i}}{\partial y}n_y+\frac{\partial M_{xy}}{\partial y}n_x+\frac{\partial M_{xy}}{\partial x}n_y\right]\delta w\,d\ell \\
&\quad -\int_{\partial\Omega}\frac{\bar{h}}{h_0}\left(Q_{x,0}n_x+Q_{y,0}n_y\right)\delta w\,d\ell = 0 \quad (2.13)
\end{aligned}$$

In order to solve the set of equilibrium equations for a *simply supported plate*, the unknown variables and the loading action are expressed in double Fourier sine series, in the form

$$w(x,y,t) = \sum_{m=1}^{M}\sum_{n=1}^{N} w_{mn}(t)\sin\left(\frac{m\pi x}{a}\right)\sin\left(\frac{n\pi y}{b}\right), \tag{2.14a}$$

$$\Delta u(x,y,t) = \sum_{m=1}^{M}\sum_{n=1}^{N} \Delta u_{mn}(t)\cos\left(\frac{m\pi x}{a}\right)\sin\left(\frac{n\pi y}{b}\right), \tag{2.14b}$$

$$\Delta v(x,y,t) = \sum_{m=1}^{M}\sum_{n=1}^{N} \Delta v_{mn}(t)\sin\left(\frac{m\pi x}{a}\right)\cos\left(\frac{n\pi y}{b}\right), \tag{2.14c}$$

$$p(x,y,t) = \sum_{m=1}^{M}\sum_{n=1}^{N} p_{mn}(t)\sin\left(\frac{m\pi x}{a}\right)\sin\left(\frac{n\pi y}{b}\right). \tag{2.14d}$$

This choice automatically fulfills the boundary conditions for a simply supported plate with in-plane free edges. By substituting them in the system (2.12), the equations relative to the m-n components become

$$\begin{aligned}\mu\frac{\partial^2 w_{mn}(t)}{\partial t^2} + \frac{E_g h^3}{6(1-\nu^2)}\left(\frac{\pi^4 m^4}{a^4}w_{mn}(t) + \frac{2\pi^4 m^2 n^2}{a^2 b^2}w_{mn}(t) + \frac{\pi^4 n^4}{b^4}w_{mn}(t)\right)\\ = \frac{\bar{h}}{h_0}C_\alpha\, {}_0^C\mathcal{D}_t^\alpha\left[-\frac{\pi m}{a}\Delta u_{mn}(\cdot) - \bar{h}\frac{\pi^2 m^2}{a^2}w_{mn}(\cdot)\right](t)\\ + \frac{\bar{h}}{h_0}C_\alpha\, {}_0^C\mathcal{D}_t^\alpha\left[-\frac{\pi n}{b}\Delta v_{mn}(\cdot) - \bar{h}\frac{\pi^2 n^2}{b^2}w_{mn}(\cdot)\right](t) + p_{mn}(t)\end{aligned} \tag{2.15a}$$

$$\begin{aligned}\frac{E_g h}{1-\nu^2}\left[-\frac{\pi^2 m^2}{a^2}\Delta u_{mn}(t) - \frac{\pi^2 n^2}{2b^2}(1-\nu)\Delta u_{mn}(t) - \frac{\pi^2 mn}{2ab}(1+\nu)\Delta v_{mn}(t)\right]\\ = \frac{2}{h_0}C_\alpha\, {}_0^C\mathcal{D}_t^\alpha\left[\Delta u_{mn}(\cdot) + \bar{h}\frac{\pi m}{a}w_{mn}(\cdot)\right](t)\end{aligned} \tag{2.15b}$$

$$\begin{aligned}\frac{E_g h}{1-\nu^2}\left[-\frac{\pi^2 n^2}{b^2}\Delta v_{mn}(t) - \frac{\pi^2 m^2}{2a^2}(1-\nu)\Delta v_{mn}(t) - \frac{\pi^2 mn}{2ab}(1+\nu)\Delta u_{mn}(t)\right]\\ = \frac{2}{h_0}C_\alpha\, {}_0^C\mathcal{D}_t^\alpha\left[\Delta v_{mn}(\cdot) + \bar{h}\frac{\pi n}{b}w_{mn}(\cdot)\right](t).\end{aligned} \tag{2.15c}$$

This problem regards only the time dependent functions $w_{mn}(t)$, $\Delta u_{mn}(t)$ and $\Delta v_{mn}(t)$, with initial conditions $w_{mn}(t) = \Delta u_{mn}(t) = \Delta v_{mn}(t) = 0$ for $t < 0$.

The system (2.15) can be numerically solved by approximating the fractional derivatives via the Grünwald-Letnikov approach, referred to in the Appendix. Let the time interval of interest $[0, T]$ be divided in s subintervals, whose amplitude is $\Delta t = t_{j+1} - t_j$ with $1 \leq j \leq s-1$. Then, preliminary calculate the $s \times s$ matrices

$$\mathbf{A}^{(\xi)} = \frac{1}{\Delta t^{\xi}} \begin{bmatrix} \omega_1(\xi) & & & \\ \omega_2(\xi) & \omega_1(\xi) & & \\ \vdots & \ddots & \ddots & \\ \omega_s(\xi) & \dots & \omega_2(\xi) & \omega_1(\xi) \end{bmatrix} = \begin{bmatrix} A_{11}^{(\xi)} & & & \\ A_{21}^{(\xi)} & A_{22}^{(\xi)} & & \\ \vdots & \ddots & \ddots & \\ A_{s1}^{(\xi)} & \dots & \dots & A_{ss}^{(\xi)} \end{bmatrix} \tag{2.16}$$

with $\omega_1 = 1$, $\omega_2 = -\xi$, $\dots$, $\omega_{\xi+1} = \dfrac{j-\xi-1}{j}\omega_j(\xi)$. If we express $f(t)|_{t=t_j} = f_j$ as the value of the generic function $f(t)$ at $t = t_j$, the discrete approximation of the system (2.15) becomes

$$\begin{aligned} &\mu \sum_{g=1}^{j+1} A_{j+1,g}^{(2)} w_{mn,g} + \frac{E_g h^3}{6(1-\nu^2)} \left(\frac{\pi^4 m^4}{a^4} + \frac{2\pi^4 m^2 n^2}{a^2 b^2} + \frac{\pi^4 n^4}{b^4} \right) w_{mn,j} \\ &\qquad = \frac{\bar{h}}{h_0} C_\alpha \left[-\frac{\pi m}{a} \sum_{g=1}^{j} A_{j,g}^{(\alpha)} \Delta u_{mn,g} - \bar{h} \frac{\pi^2 m^2}{a^2} \sum_{g=1}^{j} A_{j,g}^{(\alpha)} w_{mn,g} \right] \\ &\qquad + \frac{\bar{h}}{h_0} C_\alpha \left[-\frac{\pi n}{b} \sum_{g=1}^{j} A_{j,g}^{(\alpha)} \Delta v_{mn,g} - \bar{h} \frac{\pi^2 n^2}{b^2} \sum_{g=1}^{j} A_{j,g}^{(\alpha)} w_{mn,g} \right] + p_{mn,j} \,, \end{aligned} \tag{2.17a}$$

$$\begin{aligned} &\frac{E_g h}{1-\nu^2} \left[-\frac{\pi^2 m^2}{a^2} \Delta u_{mn,j} - \frac{\pi^2 n^2}{2b^2} (1-\nu) \Delta u_{mn,j} - \frac{\pi^2 mn}{2ab} (1+\nu) \Delta v_{mn,j} \right] \\ &\qquad = \frac{2}{h_0} C_\alpha \left[\sum_{g=1}^{j} A_{j,g}^{(\alpha)} \Delta u_{mn,g} + \bar{h} \frac{\pi m}{a} \sum_{g=1}^{j} A_{j,g}^{(\alpha)} w_{mn,g} \right] , \end{aligned} \tag{2.17b}$$

$$\frac{E_g h}{1-\nu^2}\left[-\frac{\pi^2 n^2}{b^2}\Delta v_{mn,j} - \frac{\pi^2 m^2}{2a^2}(1-\nu)\Delta v_{mn,j} - \frac{\pi^2 mn}{2ab}(1+\nu)\Delta u_{mn,j}\right] = \frac{2}{h_0}C_\alpha\left[\sum_{g=1}^{j} A_{j,g}^{(\alpha)}\Delta v_{mn,g} + \bar{h}\frac{\pi n}{b}\sum_{g=1}^{j} A_{j,g}^{(\alpha)} w_{mn,g}\right]. \quad (2.17c)$$

This is an algebraic system, from which the unknown values $w_{mn,j+1}$, $\Delta u_{mn,j}$ and $\Delta v_{mn,j}$ can be obtained as a function of the corresponding values at the previous steps, starting from null initial conditions. The complete solution, related to the m-n mode, is given by

$$\mathbf{w}_{mn,s}^T = \left[w_{mn,1}(t_1)\ w_{mn,2}(t_2)\ \ldots\ w_{mn,s}(t_s)\right],$$

$$\mathbf{\Delta u}_{mn,s}^T = \left[\Delta u_{mn,1}(t_1)\ \Delta u_{mn,2}(t_2)\ \ldots\ \Delta u_{mn,s}(t_s)\right],$$

$$\mathbf{\Delta v}_{mn,s}^T = \left[\Delta v_{mn,1}(t_1)\ \Delta v_{mn,2}(t_2)\ \ldots\ \Delta v_{mn,s}(t_s)\right].$$

2.2 Schematization of the supporting back structure

In practical applications, the panel is connected to a load-bearing back structure, whose deformation cannot be neglected in general. In particular cases, the compliance of the load-bearing structure can be tailored designed, in order to tune the dynamic response of the system and absorb/dissipate at least part of the energy from the blast wave, safeguarding the integrity of the panel.

We now consider the mechanical system schematically represented in Fig. 2, where the back structure is modelled via a lumped oscillating mass m_r, connected to the ground by means of the spring k_r in parallel with the dashpot c_r. Four kinematic variables describe the deformation in this configuration: the translation of the back structure $\tilde{w}(t)$; the out-of-plane displacement of panel $w(x,y,t)$ and the in-plane relative displacements between the external layers $\Delta u(x,y,t)$ and $\Delta v(x,y,t)$ (reference frame as in Fig. 1(a)).

The set of equilibrium equations is deduced again from Hamilton's principle (2.7).

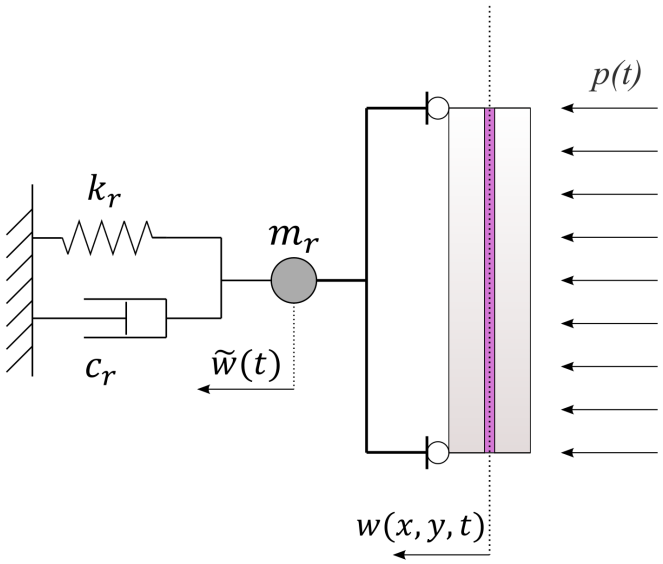

Figure 2: Laminated panel attached to a compliant load-bearing back structure, modelled as a damped spring-mass system. A time-dependent force per unit area $p(t)$ is exerted on the panel surface.

The kinetic energy $\mathcal{K}$ of (2.8) has to be complemented with the contribution of the mass m_r and shall consider that the absolute out-of-plane displacement of any point (x, y) of the plate is now $w(x, y, t) + \tilde{w}(t)$. The elastic energy $\mathcal{U}$ takes the same form (2.9), to which the part associated with k_r has to be added. The dissipation from the non-conservative forces is again given by (2.10) plus the contribution from c_r. In the work of external forces (2.11), one has now to consider $w(x, y, t) + \tilde{w}(t)$ in place of $w(x, y, t)$.

There are now four partial differential equations, that are respectively associated with each kinematic variable. The motion of the supporting back structure is governed by the equivalence

$$m_r \frac{\partial^2 \tilde{w}(t)}{\partial t^2} + \mu \int_A \left[\frac{\partial^2 w(x, x, t)}{\partial t^2} + \frac{\partial^2 \tilde{w}(t)}{\partial t^2} \right] dA + c_r \frac{\partial \tilde{w}(t)}{\partial t} + k_r \tilde{w}(t) = \int_A p(t)\, dA\,. \quad (2.18)$$

For what concerns the out-of-plane equilibrium, this reads

$$\mu\left(\frac{\partial^2 w(x,y,t)}{\partial t^2}+\frac{\partial^2 \tilde{w}(t)}{\partial t^2}\right) + \frac{E_g h^3}{6(1-\nu^2)}\left(\frac{\partial^4 w(x,y,t)}{\partial x^4}+2\frac{\partial^4 w(x,y,t)}{\partial x^2\partial y^2}+\frac{\partial^4 w(x,y,t)}{\partial y^4}\right) = \frac{\bar{h}}{h_0}C_\alpha\, {}_0^C\mathcal{D}_t^\alpha\left[\frac{\partial \Delta u(x,y,\cdot)}{\partial x}+\bar{h}\frac{\partial^2 w(x,y,\cdot)}{\partial x^2}\right](t) + \frac{\bar{h}}{h_0}C_\alpha\, {}_0^C\mathcal{D}_t^\alpha\left[\frac{\partial \Delta v(x,y,\cdot)}{\partial y}+\bar{h}\frac{\partial^2 w(x,y,\cdot)}{\partial y^2}\right](t)+p(t)\,. \quad (2.19)$$

The in-plane equilibrium of the panel is still governed by (2.12b)-(2.12c).

This set of equations can be solved by substituting the unknown functions with their double Fourier sine series (2.14) and by applying the Grünwald-Letnikov integration scheme over the time. Since the translation $\tilde{w}(t)$ does not depend on the spatial coordinates (x,y,z), it is necessary to preliminary integrate the equation (2.19) over the area of panel, so that it becomes

$$\mu\left(\Xi_{mn}\frac{\partial^2 w_{mn}(t)}{\partial t^2}+\Theta_{mn}\frac{\partial^2 \tilde{w}(t)}{\partial t^2}\right) + \frac{\Xi_{mn}E_g h^3}{6(1-\nu^2)}\left(\frac{\pi^4 m^4}{a^4}w_{mn}(t)+\frac{2\pi^4 m^2 n^2}{a^2 b^2}w_{mn}(t)+\frac{\pi^4 n^4}{b^4}w_{mn}(t)\right) = \Xi_{mn}\left\{\frac{\bar{h}}{h_0}C_\alpha\, {}_0^C\mathcal{D}_t^\alpha\left[-\frac{\pi m}{a}\Delta u_{mn}(\cdot)-\bar{h}\frac{\pi^2 m^2}{a^2}w_{mn}(\cdot)\right](t) + \frac{\bar{h}}{h_0}C_\alpha\, {}_0^C\mathcal{D}_t^\alpha\left[-\frac{\pi n}{b}\Delta v_{mn}(\cdot)-\bar{h}\frac{\pi^2 n^2}{b^2}w_{mn}(\cdot)\right](t)+p_{mn}(t)\right\}, \quad (2.20)$$

where we have set

$$\Theta_{mn}=\int_A \sin\left(\frac{m\pi x}{a}\right)\sin\left(\frac{n\pi y}{b}\right)dA, \quad (2.21a)$$

$$\Xi_{mn}=\int_A \sin^2\left(\frac{m\pi x}{a}\right)\sin^2\left(\frac{n\pi y}{b}\right)dA\,. \quad (2.21b)$$

From the subset equations (2.20) and (2.15b)-(2.15c), each mode $w_{mn}(t)$ can be found as a function of $\tilde{w}(t)$. The modes $w_{mn}(t)$ are calculated in cascade at each time step. By substituting in the equation (2.18), one finds

$$m_r \frac{\partial^2 \tilde{w}(t)}{\partial t^2} + \mu \int_A \left[\frac{\partial^2 w_{mn}(t)}{\partial t^2} \sum_{m=1}^{M} \sum_{n=1}^{N} \sin\left(\frac{m\pi x}{a}\right) \sin\left(\frac{n\pi y}{b}\right) + \frac{\partial^2 \tilde{w}(t)}{\partial t^2} \right] dA + c_r \frac{\partial \tilde{w}(t)}{\partial t} + k_r \tilde{w}(t) = \int_A p(t)\, dA\,, \quad (2.22)$$

where now $\tilde{w}(t)$ is the sole variable.

3 Loading action and constitutive properties

The loading action and the constitutive properties of interlayer are now discussed. The load is a pressure distributed on the panel surface, interpreted via Friedlander equation, which is classically used to model the effects of an explosion. For what concerns the viscoelastic properties of the interlayer, experimental data are taken from the technical literature and the fractional model is calibrated accordingly.

3.1 The blast action

The glass panel is loaded with a time dependent uniformly distributed pressure. The time history for such an action is that classified as EXV25, in accordance with the standard ISO 16933:2007 [50]. This load refers to an open arena full-scale blast test, performed by placing the target (glass panel) on a rigid frame at $R = 25\,\text{m}$ from the detonating charge, with a released energy corresponding to 100 kg of TNT. The variation in time of the action can be interpreted via Friedlander equation [22]

$$p(t) = p_r \left(1 - \frac{t}{T_d}\right) e^{-\beta \frac{t}{T_d}}\,, \quad (3.1)$$

where p_r is the peak overpressure, T_d is the time positive duration and β is the decay coefficient. The ISO 16933:2007 prescribes the peak overpressure $p_r = 80\,\text{kPa}$ and the positive impulse $i_r^+ = 380\,\text{kPa·ms}$, while the other parameters are obtained as a

function of the "scaled distance" [51]. In particular, $W_{\rm TNT} = (1.7 \cdot 100)\,\mathrm{kg}$ is taken as equivalent mass of charge, where the coefficient 1.7 is needed to consider the ground reflection (surface burst): since the energy is concentrated inside a hemispherical volume, it consequently results almost doubled. Hence, the scaled distance becomes

$$Z = \frac{R}{W_{\rm TNT}^{1/3}} = \frac{25}{(1.71 \cdot 100)^{1/3}} = 4.51\,\mathrm{kg/m^{1/3}}\,. \tag{3.2}$$

Empirical formulae have been proposed in order to get the time positive duration T_d as a function of the variable Z. Because of its optimal agreement with experimental results provided by Kingery and Bulmash [52], the expression by Kinney and Graham [23] is here used, which reads

$$T_d = W_{\rm TNT}^{1/3} \cdot \frac{980\left[1+\left(\dfrac{Z}{0.54}\right)^{10}\right]}{\left[1+\left(\dfrac{Z}{0.02}\right)^{3}\right]\cdot\left[1+\left(\dfrac{Z}{0.74}\right)^{6}\right]\cdot\sqrt{\left[1+\left(\dfrac{Z}{6.9}\right)^{2}\right]}} = 12.7\ \mathrm{ms}\,. \tag{3.3}$$

From the equation

$$i_r^+ = \int_0^{T_d} p_r\left(1-\frac{t}{T_d}\right)e^{-\frac{\beta}{T_d}t}\,dt = p_r T_d\left[\frac{1}{\beta}-\frac{1}{\beta^2}(1-e^{-\beta})\right], \tag{3.4}$$

the decay coefficient $\beta = 0.95$ is then calculated. The time history for such a pressure load is represented in Fig. 3.

3.2 Viscoelastic interlayers

The glass plies are bonded together by a thin polymeric interlayer, whose viscoelastic behavior is characterized by its relaxation function. In the bi-logarithmic stress-time plane, the shape of this curve is constituted by two pseudo-linear branches, which are connected by a transition zone where the stress decreases. The time domain can be very wide but, since a generic blast load presents a duration of order $T_d \sim 0.01\,\mathrm{s}$, for most commercial materials used as interlayers only the extremal left hand side

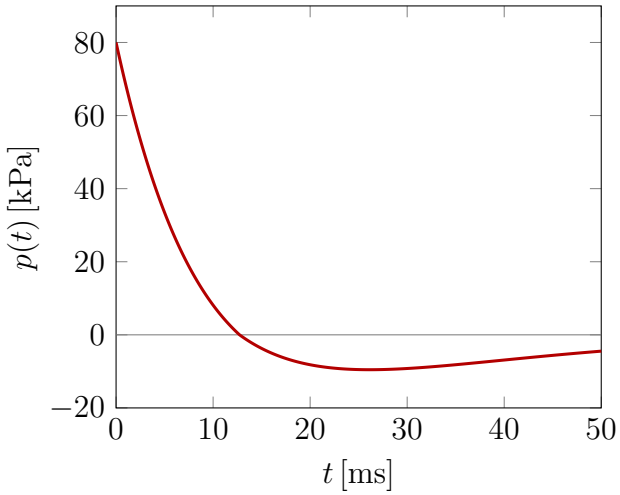

Figure 3: Time dependent pressure loading on the panel surface. The time history follows the classical Friedlander equation, whose parameters are fixed in agreement with ISO 16933:2007 [50].

branch of such curve is of importance.

At very small temporal scales, the mechanical response of a polymer may be determined by means of Dynamic Mechanical Analyzers (DMA) [53]. This kind of testing apparatus shall necessary handle the pristine polymer, which is subjected to a periodic load/deformation with preset amplitude and frequency. However, in order to be used as cohesive interlayer, the polymer has to be laminated at high temperatures and pressures in autoclave, so that its viscoelastic properties get modified. Therefore, the most reliable experimental alternative is to perform static tests directly on laminated glass samples and extrapolate the relaxation function for small time values. For practical reasons (inertia of the testing machine, feasibility), the observation period is limited to an interval varying from a minimum of a few seconds to a maximum of a few weeks at most. The extrapolation to very small and very large time scales can be done on the basis of Time-Temperature Superposition (TTS) principle, according to which a variation of the testing temperature is associated with a variation of the time scale for the effects of viscosity.

In practice, if the relaxation curve at the reference temperature $\mathcal{T}_0$ is expressed by $R = R_{\mathcal{T}_0}(t)$, at the temperature $\mathcal{T}$ it shall be $R = R_{\mathcal{T}}(t) = R_{\mathcal{T}_0}(t/a_{\mathcal{T}})$. The most commonly accepted model relies upon the Williams Landel Ferry (WLF) equation

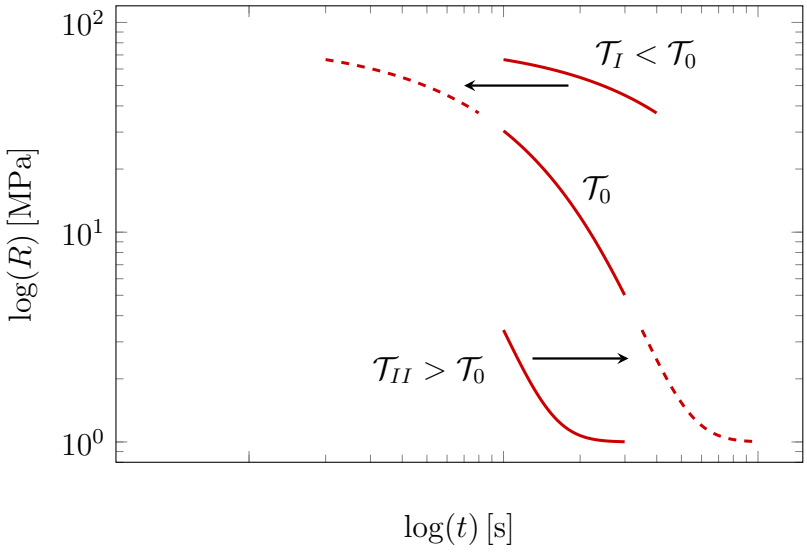

Figure 4: Time-Temperature Superposition (TTS) principle used to obtain the relaxation function $R = R_{\mathcal{T}_0}(t)$ at the reference temperature $\mathcal{T}_0$, by shifting the experimental curves (continuous line), measured at the temperatures $\mathcal{T}_I < \mathcal{T}_0$ and $\mathcal{T}_{II} > \mathcal{T}_0$.

[54], which determines the time shift $\log(a_{\mathcal{T}})$ as a function of the environmental temperature $\mathcal{T}$ and a reference temperature $\mathcal{T}_0$, in the form

$$\log(a_{\mathcal{T}}) = \frac{-C_1(\mathcal{T} - \mathcal{T}_0)}{C_2 - (\mathcal{T} - \mathcal{T}_0)}\,, \tag{3.5}$$

where C_1 and C_2 are experimental constants. Hence, several tests can be performed within the same reference time interval at different temperatures; the curves are then shifted to find other branches of the relaxation curve at the reference temperature $\mathcal{T}_0$. Such procedure can be conceptualized as in Fig. 4: the curve obtained at $\mathcal{T}_I < \mathcal{T}_0$ ($\mathcal{T}_{II} > \mathcal{T}_0$) is left-shifted (right-shifted) in the bi-logarithmic stress-time plane.

The resulting curve is usually of the type represented in Fig. 5. For most materials used in the glass industry, the transition zone is located in a time interval varying from a few seconds to a few days. Therefore, at very short time scales, such as those representative of a bomb-blast event, the branch of interest is certainly the first branch (left hand side of the graph). This can be effectively fitted by a power law (linear trend in the bi-logarithmic scale) which, following the usual notation of fractional viscoelasticity recalled in the Appendix, can be expressed in the form

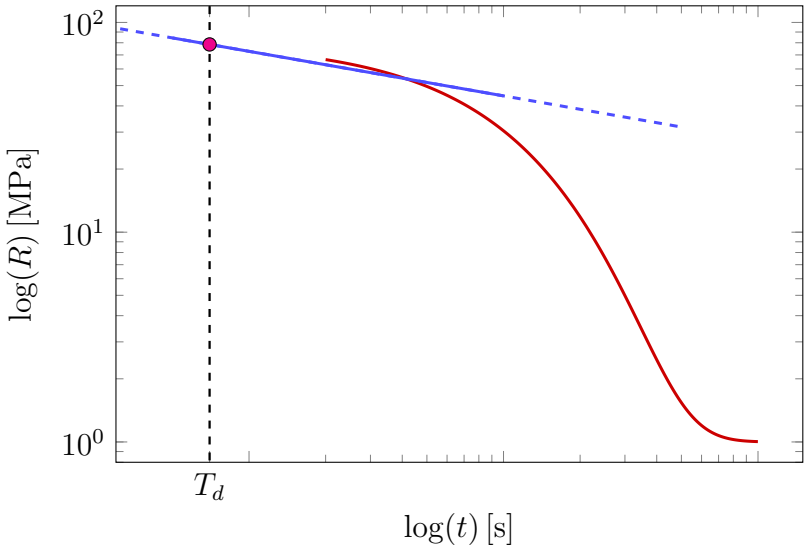

Figure 5: Qualitative plot of a typical relaxation function $R(t)$. The first branch is fitted by a power law (straight line), which allows to analytically extrapolate the values at time-scales of the same order of the characteristic load duration T_d.

$$R(t) = \frac{C_\alpha}{\Gamma(1-\alpha)} t^{-\alpha}, \tag{3.6}$$

where $\Gamma(\cdot)$ is the Euler's Gamma function and C_α [MPa s$^\alpha$] is a dimensional coefficient. In the bi-logarithmic graph, also indicated in Fig. 5, the non-dimensional coefficient α represents the slope of the line, while C_α is the value of the function at $t = 1\,\mathrm{s}$. In general, this linear trend shall be extrapolated to cover time scales of the same order of the blast characteristic duration T_d.

In this article, three different interlayers, respectively denoted as $\mathcal{A}$, $\mathcal{B}$ and $\mathcal{C}$, will be considered, which cover a wide range of viscoelastic coupling for the glass plies. They correspond to three relaxation curves experimentally measured by Biolzi et al. [55] for three different materials: polyvinyl butyral (PVB) at 50 °C; ionoplast SentryGlas (SG) at 50 °C; a high performance plasticized PVB (commercially known as DG41) at 15 °C. The measured trend of the relaxation curves is linear in practice in the bi-logarithmic plane; hence, they can be well interpreted by a power law of the type (3.6). The corresponding fractional viscoelastic parameters (α and C_α), obtained by the interpolation of the raw data, are reported in Table 1.

Interlayer	Sample	α	C_α [MPa s$^\alpha$]
$\mathcal{A}$	PVB at 50 °C	0.155	0.474
$\mathcal{B}$	SG at 50 °C	0.117	9.409
$\mathcal{C}$	DG41 at 15 °C	0.117	84.138

Table 1: Properties of polymeric interlayers, which exhibit a power law trend according to the experimental measurements by Biolzi et al. [55] in the representative time interval. The corresponding fractional viscoelastic parameters α and C_α have been obtained by interpolating the raw data.

At this point, however, a question of paramount importance should be raised. Is it possible to interpolate the raw data with a power law and extrapolate the results at very low time scales? The answer is positive if and only if the transition zone occurs later than the observation interval, i.e., if the branch that is being measured is the left hand side pseudo-linear branch of Fig. 5. In general, this requirement is satisfied, but not always. There can be particular materials for which the transition zone, at relatively high temperatures, occurs for times of the order of 1 s, which is smaller that the time needed to strain the specimen in a direct relaxation test (of the order of some seconds). In this case, the experimental measurement would provide a pseudo-linear curve in the bi-logarithmic plot, but this would correspond to the right hand side of the whole relaxation curve.

To illustrate, we have reported the whole relaxation curve for the material SG at 50 °C [55] by using the (3.6). The corresponding graph is reported in Fig. 6, where the measured points are marked with dots, together with the interpolating straight line obtained with the parameters of Table 1. It thus becomes clear that this line corresponds to the right hand side pseudolinear branch. Consequently, the use of this approximation in the model would correspond to a noteworthy underestimation of the stiffness of the polymer and, hence, of the degree of coupling of the glass plies.

In general, the measured response at relatively high temperatures (of the order of 50 °C) should be associated with the right hand side pseudolinear branch of the

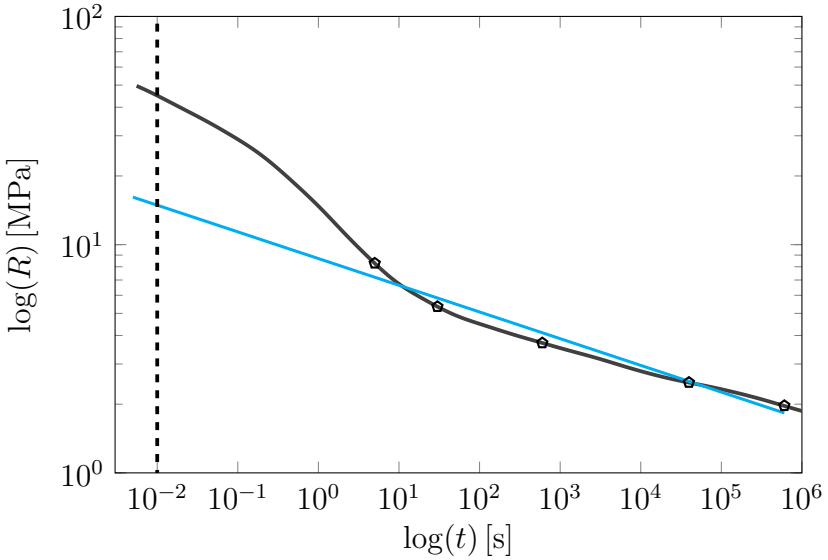

Figure 6: Relaxation function for the polymer SG at 50 °C: complete curve obtained with the Time-Temperature Superposition principle (gray line); directly measured points (dots); fitting of the measured points with a power law (cyan line).

relaxation curve (in the bi-logarithmic representation). For the cases considered in Table 1, this is indeed the situations for materials $\mathcal{A}$ and $\mathcal{B}$. Despite this, in the following we will continue to refer to the viscoelastic parameters shown in the Table 1, having in mind that materials $\mathcal{A}$ and $\mathcal{B}$ should be considered as theoretical reference cases, not directly associable with the responses of the PVB and the SG at 50 °C, respectively. On the contrary, the parameters for materials $\mathcal{C}$ actually correspond to the left hand side tail of the relaxation curve and, hence, indicate the real condition. It was decided to consider these data because they provide a wide range of viscoelastic responses, which can be useful for showing the potential of the theoretical model in a substantial variety of conditions.

4 Numerical Experiments

The following numerical experiments investigate the dynamic response of a simply supported laminated glass plate. Three different-in-type interlayers are taken into account, in order to define how they can differently affect the bending stress in the

glass. The effect of a compliant back structure is also discussed.

The laminated plate, schematically represented in Fig. 1, is composed of two identical external layers made of glass, whose dimensions are $a \times b \times h_i = 1 \times 1 \times 0.01\,\mathrm{m}^3$, $i = 1, 2$, with Young's modulus $E_g = 70\,\mathrm{GPa}$, Poisson's ratio $\nu = 0.25$ and density $\rho = 2500\,\mathrm{kg/m}^3$. They sandwich an interlayer of thickness $h_0 = 2.28\,\mathrm{mm}$ and density $\rho_0 = 1000\,\mathrm{kg/m}^3$, for which we consider three different materials. Their constitutive properties are indicated in Table 1: $\alpha = 0.155$, $C_\alpha = 0.474\,\mathrm{MPa\,s}^\alpha$ (material $\mathcal{A}$); $\alpha = 0.117$, $C_\alpha = 9.409\,\mathrm{MPa\,s}^\alpha$ (material $\mathcal{B}$); $\alpha = 0.117$, $C_\alpha = 84.138\,\mathrm{MPa\,s}^\alpha$ (material $\mathcal{C}$). The laminated plate is subjected to a uniformly distributed pressure depending on time through Friedlander equation (3.1), whose parameters have been set in Section 3.1. The possible presence of one deformable supporting structure is schematized as in Fig. 2.

4.1 Dynamic response of a plate with rigid supports

In the Fourier expansions (2.14), the asymmetric modes are null because the problem is symmetric: we first attempt at considering modes $m = 1, 3$ and $n = 1, 3$ only. Fig. 7 reports the displacement components $w_{mn}(t)$ as a function of time for an interlayer of type $\mathcal{A}$. It is clear that first mode $w_{11}(t)$ is dominant, while the second modes $w_{13}(t) \equiv w_{31}(t)$ provide for oscillations of amplitude two orders of magnitude smaller. The graph of mode $w_{33}(t)$ is not reported because of negligible amplitude. This example confirms that a truncation to the third order in the Fourier expansion does not cause appreciable loss of precision. The same conclusion is expected to be valid also for the other interlayers, which are stiffer than material $\mathcal{A}$.

The state of stress in the glass is measured by the component σ_{xx}, evaluated on the external surface of the internal ply (the one not directly invested by the pressure wave), in correspondence of the center $(x, y) = (a/2, b/2)$. The corresponding time history is plotted in Fig. 8 for the softest material $\mathcal{A}$, which is juxtaposed to the graphs corresponding to the layered limit (free-sliding plies, $C_\alpha = 0\,\mathrm{MPa\ s}^\alpha$) and monolithic limit (rigid shear coupling of the plies, $C_\alpha \to \infty\,\mathrm{MPa\ s}^\alpha$). The Figure shows that an interlayer of the type $\mathcal{A}$ provides results close to the layered limit: therefore the stress is due to the bending contribution. The maximum tensile peak is approximately 140 MPa; the compression peak is of the same order.

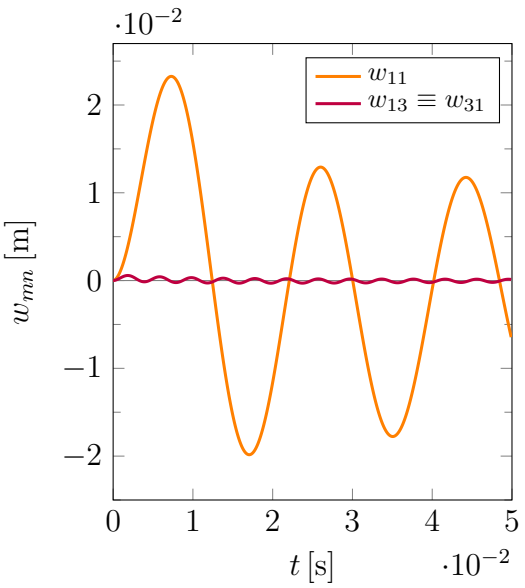

Figure 7: Vibration of a glass plate laminated with an interlayer of the type $\mathcal{A}$, simply supported along its edges and subjected to the blast force $p(t)$. The motion is decomposed in the fundamental modes of vibration $w_{mn}(t)$.

Remarkably, observe that there is a slight compression at the center of plate, occurring during the very first instants ($\sim 10^{-3}$ s). This is the most evident at the layered limit, for which it is approximately 10 MPa, while it decreases as the shear coupling of the glass plies increases, being minimal at the monolithic limit. The initial compression is due to the counter-inflection of panel in a neighborhood of its center. This is the most compliant region of the plate, which is consequently the most restrained by the effect of the inertia when it is impacted by the blast wave. Indeed, at the beginning of the deformation process, the bending shape of the plate is of the type represented in Fig. 9, where the change of curvature is evident. In general, the entity of the counter-inflection does not appear relevant for the structural integrity of the panel. However, for representative values of the key parameters (thickness of the glass plies, initial peak pressure), the dynamic response may be such that the bending failure does not start in correspondence of the center, but at the borders of the panel [56].

Observe that, since the stress distribution is linear through the thickness, the maximum and minimum values are certainly located on the surfaces of each plies. In

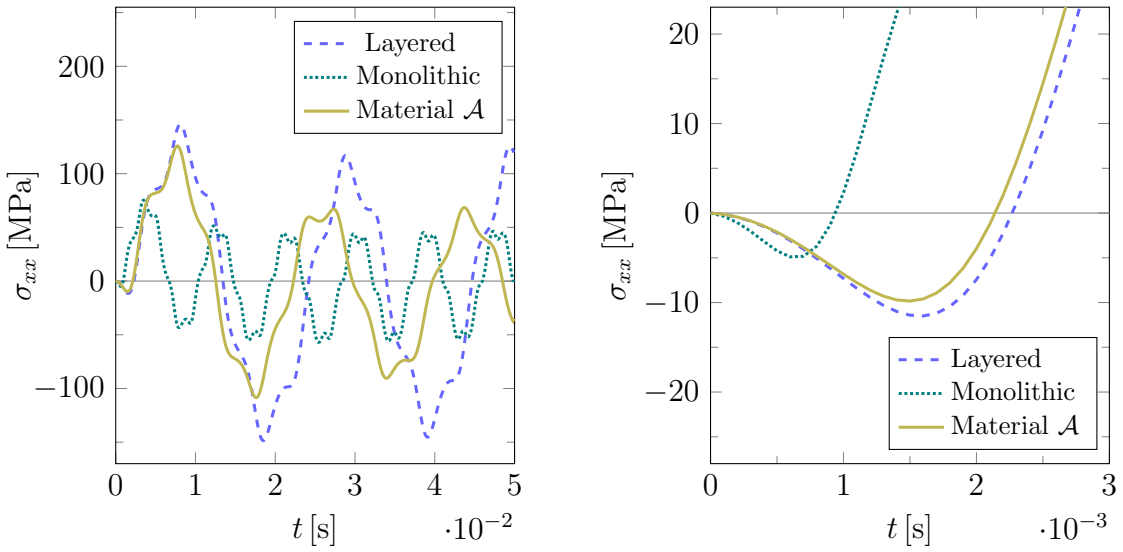

(a) (b)

Figure 8: Stress component σ_{xx} evaluated at the centre of ply 2 at $z = -h/2$. The plate is laminated with an interlayer of the type $\mathcal{A}$, it is simply supported along its edges and subject to the blast pressure $p(t)$. The corresponding solution is compared with the layered and monolithic limits. (a) Extended time interval $(0 - 5 \cdot 10^{-2}\,\mathrm{s})$; (b) detail in the first instants of loading $(0 - 3 \cdot 10^{-3}\,\mathrm{s})$.

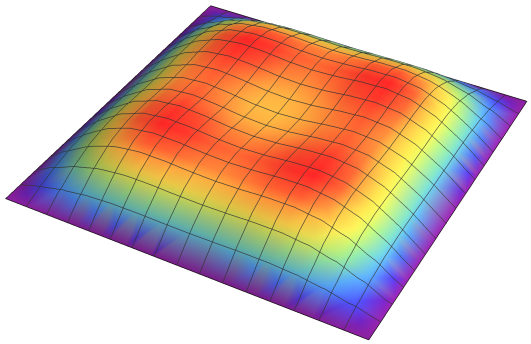

Figure 9: Qualitative deformed shape of a panel just after being impacted by the blast wave. There is a central region of counter-inflection due to the effects of the inertial forces on the plate.

Fig. 10(a), the four points A, B, C and D are schematically indicated in correspondence of the centers of the four surfaces of the glass plies; for an interlayer of the type $\mathcal{A}$, the corresponding σ_{xx} is represented as a function of time in Fig. 10(b). The

external points A and D are those subjected to the highest stresses in absolute value, because here the bending and membrane contribution sum up. On the contrary, the membrane contribution is opposite to the bending contributions in correspondence of the internal points B and D. At the layered limit, where the membrane stress is null, the stress at the external points shall be opposite to that at the internal points. Hence, the graphs of Fig. 10(b) indicate that the interlayer of the type $\mathcal{A}$ provides a condition close to the layered limit.

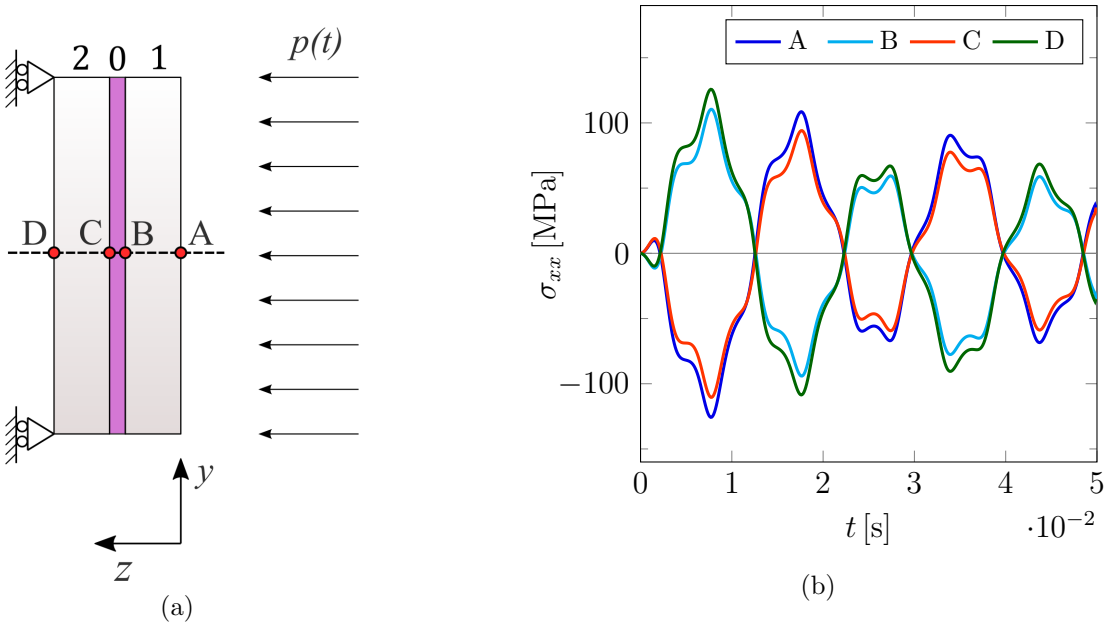

Figure 10: Stress component σ_{xx} evaluated at the centre of ply 1 and ply 2 at $z = \pm h/2$. The plate, laminated with an interlayer of the type $\mathcal{A}$, is simply supported along its edges and it is subject to the blast pressure $p(t)$. (a) Schematic representation of the loaded sandwich plate, with indication of the points of measure. (b) Stress-time graphs.

In Fig. 11, we show the time histories of σ_{xx}, evaluated at point D of Fig. 10(a) (centre of the external surface of the second ply), when the interlayer is of the type $\mathcal{B}$ or $\mathcal{C}$. It is evident that now the response is closer to the monolithic limit, because C_α is higher than for material $\mathcal{A}$ and the interlayer is stiffer. Both solutions provide for stress peaks of the same order. The main difference is represented by the frequency of oscillation: the higher is C_α, the higher the frequency is. For material $\mathcal{C}$, the

solution in practice overlaps with the monolithic limit. Of course, this response is consequent to high frequency excitations, as in the case of a bomb-blast event; at low excitation frequencies the viscous component may play a dominant role. In fact, one can observe from Fig. 11(b) that even for material $\mathcal{C}$ the structural response is shifted with respect to the monolithic limit.

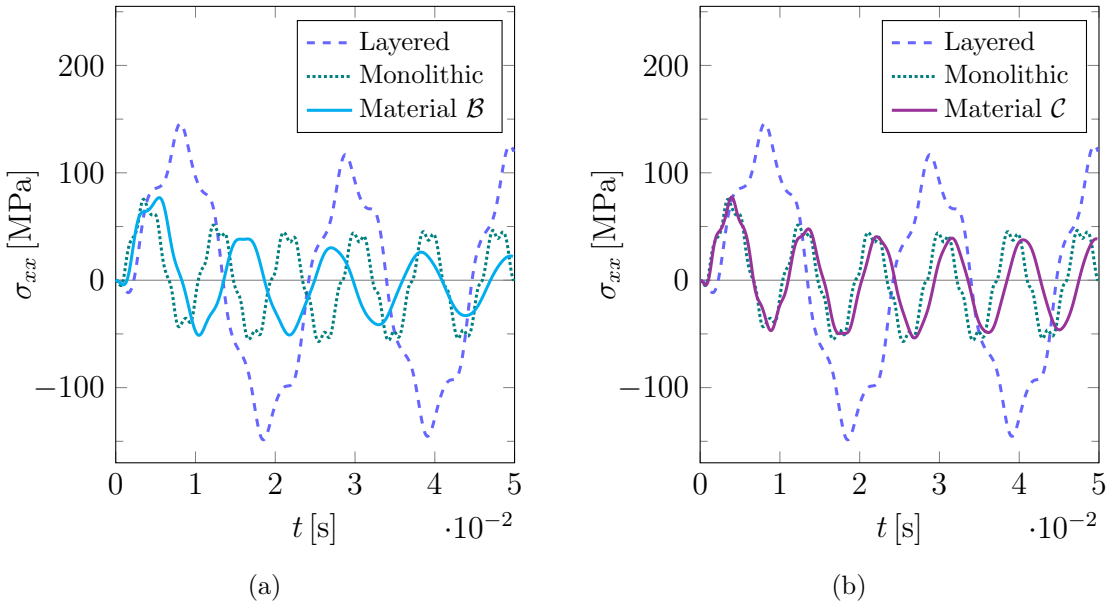

Figure 11: Stress component σ_{xx} evaluated at the centre of ply 2 at $z = -h/2$. The plate is simply supported along its edges and it is subject to the blast pressure $p(t)$. The solution is compared with the layered and monolithic limit. (a) Interlayer of type $\mathcal{B}$. (b) Interlayer of type $\mathcal{C}$.

The contour plot in Fig. 12(a) represents the distribution of the shear stress in the interlayer, calculated as $\sqrt{\tau_{xz,0}^2 + \tau_{yz,0}^2}$ [MPa]. The maximum values are located at the midpoints of the edges, whereas the shear is null at the corners and at the center. At the point $(x, y) = (0, b/2)$, highlighted by a black dot, the shear stress $\tau_{xz,0}$ is plotted as a function of time in Fig. 12(b) for the three considered interlayers. Material $\mathcal{C}$ presents the highest viscoelastic coefficient C_α; hence, it provides for the highest stress peak. For the most compliant material $\mathcal{A}$ (C_α very low), the stress peak is approximately reduced of one order of magnitude. Although there is not a proportional relation between C_α and the magnitude of the stress, it is clear that the

stiffer the interlayer, the higher the shear stress peak is.

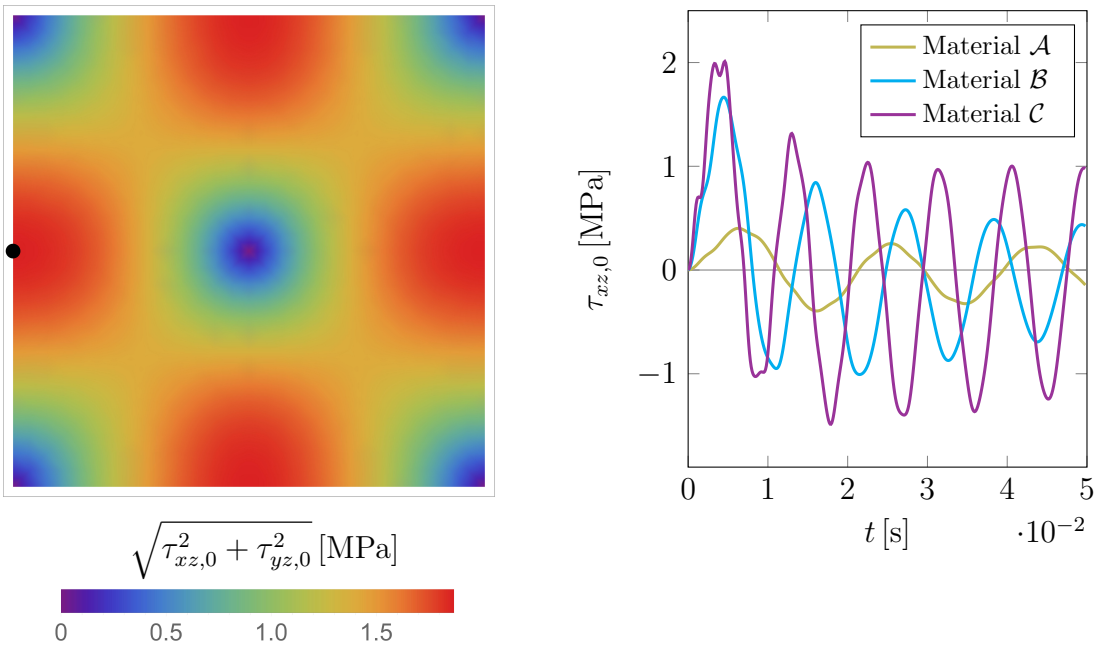

(a) (b)

Figure 12: Shear stress in the interlayer. (a) Contour plot. (b) Stress $\tau_{xz,0}$, calculated in correspondence of the midpoint of the edge (black dot), as a function of time.

In order to understand what is the contribution due to the hereditary memory of viscoelasticity for the interlayer, it is interesting to compare the previous results in terms of the stress σ_{xx} in the glass, with numerical experiments for perfectly elastic interlayers. Recall that all the relaxation functions are assumed to be power laws that fit the experimental data[1] provided by Biolzi et al. [55]. In the bi-logarithmic plots of Fig. 13, these are represented by inclined straight lines, which interpolate the experimental points, highlighted with circles in the same figure. An equivalence with an elastic material (quasi-elastic approximation [29, 57]), can be done by considering for it the shear modulus in the relaxation curve that corresponds to the characteristic duration of the action. Therefore, the elastic behavior of each interlayer is determined by drawing a horizontal line, corresponding to $\alpha = 0$, which intersects the relaxation

[1] As indicated in Section 3.2, this correspondence is *formally* assumed.

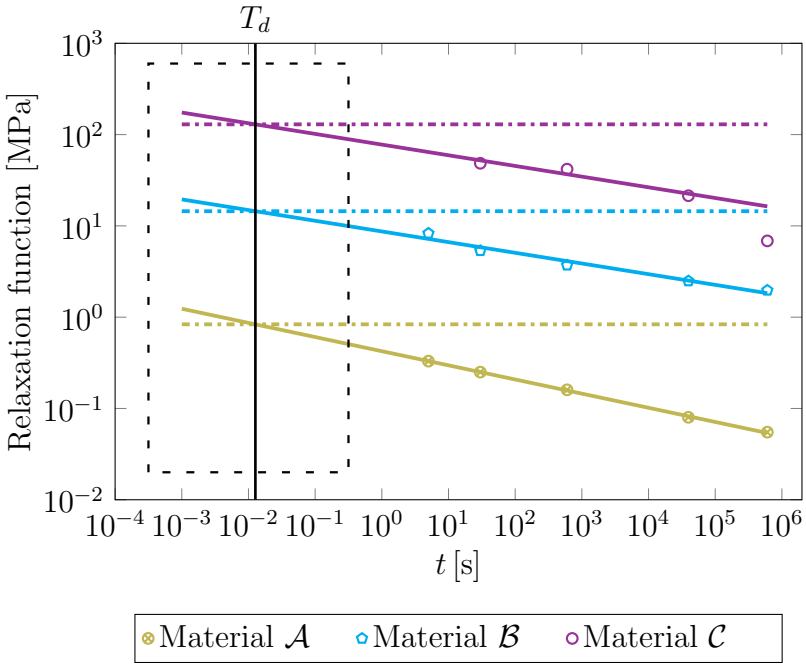

Figure 13: Relaxation functions plotted for the interlayers considered in [55]. Extrapolation with a power law (continuous lines in the bi-logarithmic scale) and elastic approximation (horizontal dash-dotted lines), by considering the secant shear modulus at $t = T_d = 1.27 \cdot 10^{-2}\,\mathrm{s}$, for materials $\mathcal{A}$, $\mathcal{B}$ and $\mathcal{C}$.

function at $t = T_d$, where $T_d = 1.27 \cdot 10^{-2}\,\mathrm{s}$ is the time duration of the positive blast pressure, as per Friedlander equation (3.1). In conclusion, the elastic limit is denoted by setting $R(t) = \hat{C}_0$ that, for the cases at hand, takes the value: $\hat{C}_0 = 0.835\,\mathrm{MPa}$ for material $\mathcal{A}$; $\hat{C}_0 = 14.484\,\mathrm{MPa}$ for material $\mathcal{B}$; $\hat{C}_0 = 129.516\,\mathrm{MPa}$ for material $\mathcal{C}$.

The results to be compared are reported in Fig. 14 for the three considered interlayers. In all the cases, there is a good superimposition between viscoelastic and elastic cases for what concerns the first peak. When considering the response in a broader time interval, the difference is minimal when considering material $\mathcal{C}$, the stiffest of all, inasmuch the monolithic limit is attained. Materials $\mathcal{A}$ and $\mathcal{B}$ provide a similar response: the dissipation provided by the viscous component decreases the magnitude of the successive peaks and slightly increases the frequency of oscillations. When the interlayer is of type $\mathcal{A}$, the sandwich is more compliant; hence, there are less oscillations within the considered time interval if compared with the other materials.

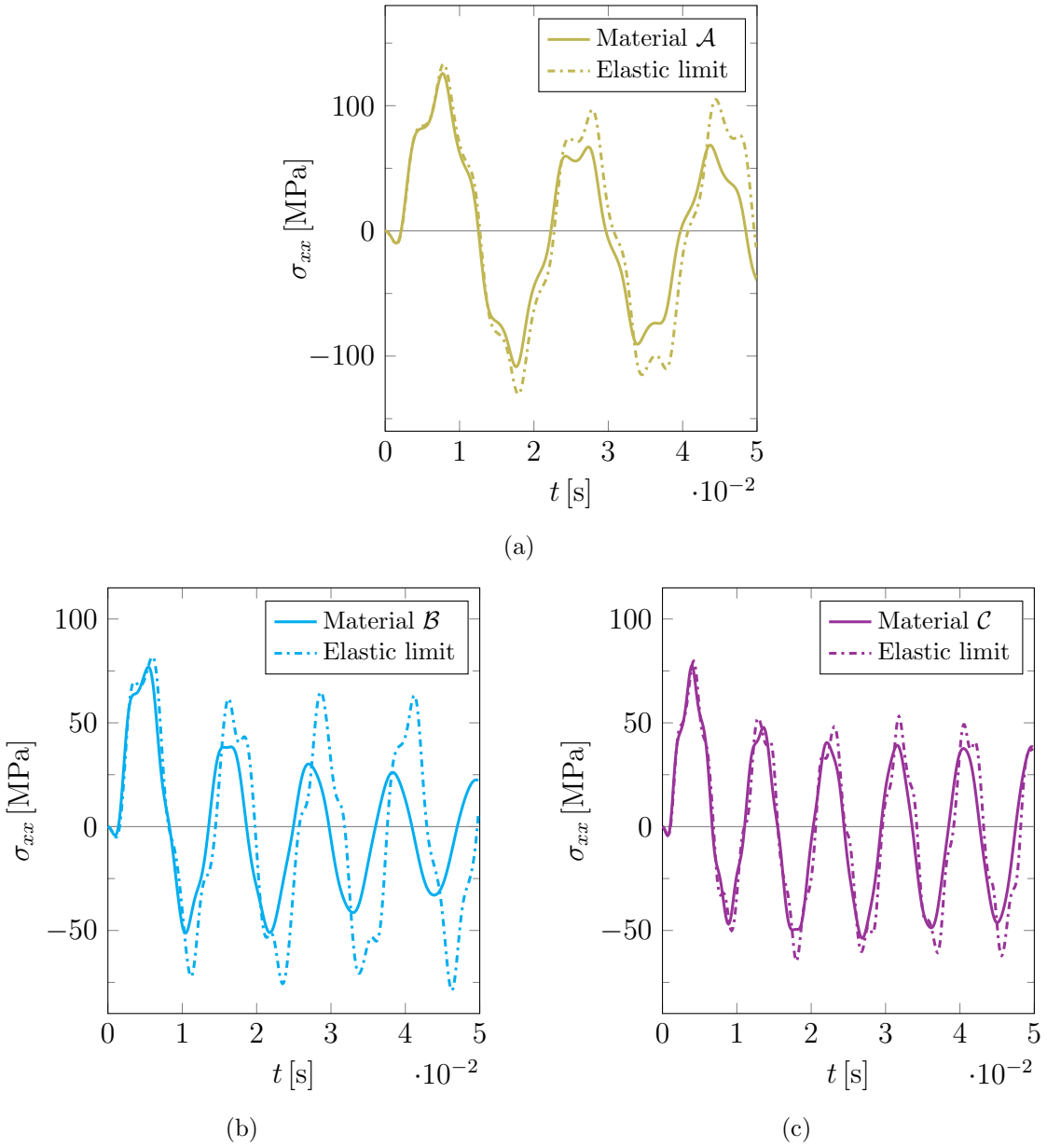

Figure 14: Stress component σ_{xx} evaluated at the centre of ply 2 at $z = -h/2$. The plate is simply supported along its edges and it is subjected to the blast pressure $p(t)$. The corresponding solutions are compared with the elastic approximation. (a) Interlayer of type $\mathcal{A}$; (b) interlayer $\mathcal{B}$; (c) interlayer $\mathcal{C}$.

Stress component σ_{xx} evaluated at the centre of ply 2 in $z = -h/2$. The plate is simply supported along its edges and it is subjected to the blast force $p(t)$. The

solution is compared to the layered and monolithic limit. (a) Interlayer of type $\mathcal{B}$. (b) Interlayer of type $\mathcal{C}$.

Stress component σ_{xx} evaluated at the centre of ply 2 in $z = -h/2$. The plate is simply supported along its edges and it is subjected to the blast force $p(t)$. The interlayer of type $\mathcal{A}$ is employed, so that the corresponding solution is compared to the layered and monolithic limit. (a) Extended time interval (0-$5 \cdot 10^{-2}$ s); (b) detail of the first instants (0-$3 \cdot 10^{-3}$ s

4.2 Effects of the supporting back structure

With reference to the simple model of Fig. 2, proposed in Section 2.2, the influence of the supporting back structure is now investigated. In particular, the following three cases are distinguished for the sake of comparison.

i. **Rigid structure.** This is the limit case $k_r \to \infty$, providing for a rigidly-borne panel. The blast wave totally transfers its energy to the panel, which responds through its deformation.

ii. **Simply supported beam.** The glass panel can be fixed to a frame composed of transoms and mullions. We assume an equivalent simply supported beam, whose cross-sectional inertia is $I = 42\,930 \cdot 10^{-8}\,\mathrm{m}^4$ with mass per unit length $\bar{m}_b = 79.4\,\mathrm{kg/m}$ (standard profile IPE A 500 UNI 5398). By setting $E_s = 210\,\mathrm{GPa}$ for steel, the spring stiffness in the model is set to be $k_r = 48E_sI/L^3 = 67.614 \cdot 10^3\,\mathrm{N/m}$ where $L = 4\,\mathrm{m}$. Assuming the shape function $\Upsilon(x) = 4(x/L)(x/L-1)$ for its deformation, the effective lumped mass results to be $m_r = \bar{m}_b \int_0^L \Upsilon(x)^2\,dx \simeq 169.387\,\mathrm{kg}$.

iii. **Pre-tensioned cable.** A back structure made of multiple cables exhibits the maximum compliance, which enhances its capacity to absorb energy from an impulsive load. We set $N_0 = 300\,\mathrm{kN}$ as the tensile force in a cable of length $L = 4\,\mathrm{m}$, so that $k_r = 2N_0/(L/2) = 150\,\mathrm{kN/m}$. In order to consider the weight of the fixing devices besides the self-weight of the cable, the considered mass is $m_r = 50\,\mathrm{kg}$, but ballast may be artfully added if advantageous.

In all the aforementioned cases, the dissipation of the back structure is interpreted through a dashpot with a damping coefficient $c_r = 0.03 \cdot 2\sqrt{m_r k_r}$ (damping ratio of 3 %). This is the classical approach, even if a fractional viscoelastic dissipator (spring-pot) could have been used. We consider in detail only the case in which the interlayer is made of material $\mathcal{A}$, which is the most interesting one because the other materials provide results close to the monolithic limit.

The displacement of the back structure is plotted in Fig. 15(a) as a function of time for the two cases of simply supported beam and pre-tensioned cable. Since their fundamental period of vibration is much higher than the interval of observation, comparable with the characteristic duration of the blast wave, none of the graphs completes a period. The contribution from stiffness and inertia induces a slower deformation in the simply supported beam than in the pre-tensioned cable. The more compliant is the load-bearing structure, the less is its resistance in terms of stiffness: the blast action is mainly equilibrated by the inertial contribution.

The time history in terms of stress σ_{xx} and out-of-plane deflection w, evaluated at point D of Fig. 10(b), are represented in Fig. 15. It is clear that, as expected, a compliant back structure substantially contributes to reduce the stress and deflection. For a back structure formed by a simply supported beam, the solution is intermediate between those corresponding to the rigid support and the pre-tensioned cable. The condition of rigid support is clearly the worst of all; using a compliant cables approximately halves the stress in the glass. If on the one hand a compliant back structure may safeguard the glass integrity, on the other hand the resulting large displacements may be incompatible with the design serviceability limit states.

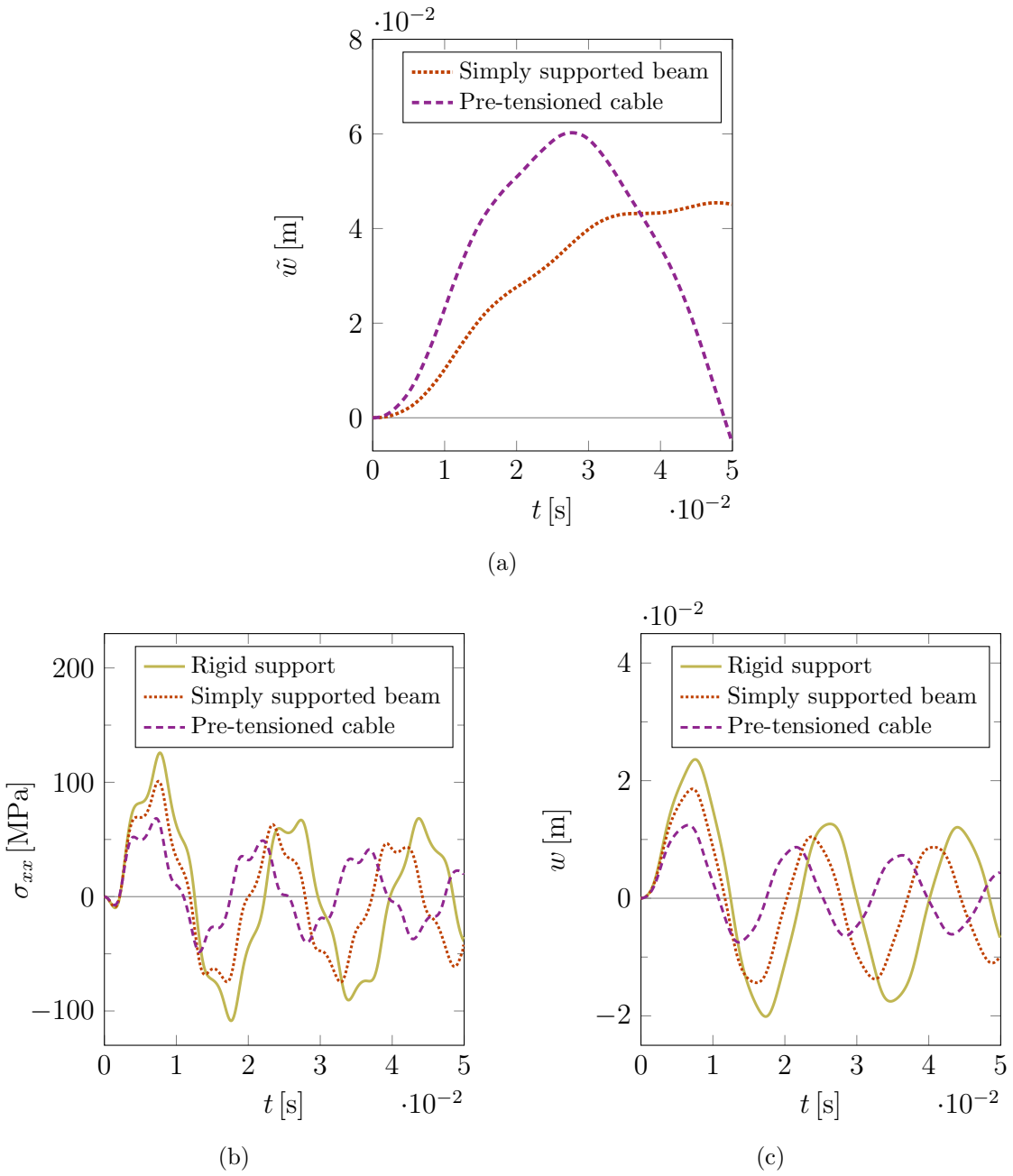

Figure 15: Comparison between different back structures: rigid support, simply supported beam and pre-tensioned cable. The panel is laminated with an interlayer of type $\mathcal{A}$ and it is subject to the blast pressure $p(t)$. (a) Displacement of the back structure $\tilde{w}$. (b) Stress components σ_{xx} at the centre of ply 2 at $z = -h/2$. (c) Out-of-plane deflection w at the centre of the plate.

5 Conclusions

The following conclusions summarize i) the novelty of the model, ii) the major results and iii) possible further developments.

A structural model for laminated glass plates has been proposed and applied under impulsive loading conditions consequent to a paradigmatic explosive event. The case study is represented by a three-layered plate, where two elastic glass plies sandwich a thin polymeric foil without bending capacity, but sufficient to provide the shear coupling of the glass plies. The novelty consists in the fractional constitutive model used for the viscoelastic interlayer. This choice appears natural because experimental results have provided a wealth of evidence that the corresponding relaxation/creep functions are power laws at small temporal scales, comparable with the characteristic duration of the pressure wave consequent to the explosion. If compared with the more classic viscoelastic description via Prony series, the fractional approach is more straightforward and computationally advantageous, since only two parameters are needed to characterize the material response. The numerical integration scheme for the fractional model does not present any additional difficulty with respect to the classical approach.

The laminated glass plate, simply supported at the borders, has been subjected to an impinging pressure varying with time according to Friedlander wave form. The numerical experiments have accounted for three different polymeric interlayers, so to obtain a wide spectrum of dynamic responses, ranging between the theoretical layered and monolithic limits. The time histories of bending stress and deflection have been compared with those resulting from the quasi-elastic approximation, according to which the interlayer is a linear elastic material, characterized by the secant elastic modulus corresponding to the characteristic duration of blast impulse. In general, the first stress peak is not qualitatively affected by the viscous dissipation from the interlayer, which however significantly lowers the values of the subsequent peaks. The effect of the load-bearing back structure has been considered by means of a lumped oscillating mass connected in series with the panel a spring/dashpot unit. A very compliant back structure, made e.g. of cables, can decrease the stress in the plate because it absorbs part of the energy transmitted by the impinging blast wave, but

the resulting deflection increases and may be incompatible with the serviceability limit states of design.

The greatest limitation of this work is represented by the assumption of linear elastic model à la Kirchhoff-Love for the glass plates, therefore neglecting the geometric non-linearities, which certainly play a role under high deformations. Further developments should consider the behaviour of multi-laminates, with more than one viscoelastic interlayer, widely used in explosion-resistant façades for their remarkable post-glass-breakage capacity. Insulating glass units, where two or more glass panes isolate one or more gas-filled chambers, require an ad hoc modelling, because the coupling between the panes occurs through the internal pressure of the trapped gas. All the models for the structural types listed above assume that the glass remains sound after the explosion, but the post-glass-breakage behaviour of the laminate will certainly have to be considered in the design phase. This aspect has not even been touched upon here, since it requires a specific description of the cohesive forces bonding the glass shards to the interlayer, which goes far beyond the scope of this article. Nonetheless, this study confirms that the viscoelastic model based on fractional calculus can be conveniently used in complex structures such as layered plates, not only without additional complications, but with great simplifications compared to other approaches.

Acknowledgements. Luca Viviani greatefully acknowledges the funding by Maffeis Engineering SpA of his scholarship to attend the PhD program in Industrial Engineering at the University of Parma.

A Appendix: Fractional calculus in viscoelasticity

The characterization of the viscoelastic properties via fractional calculus is particularly efficient for those stressed solids whose response can be well fitted by a power law. This is the case for a wide range of materials [7], such as rubber, steel and polymers, at least in a given time interval of observation. Specifically, under the stress history $\tau(t) = \tau_0 \, \mathcal{H}(t)$, where $\mathcal{H}(t)$ is the unit Heaviside step function and $\tau_0 = 1\,\mathrm{Pa}$

the reference unitary shear stress, it is convenient to express the corresponding strain $J(t)$ as a *creep function* of the form

$$J(t) = \frac{t^\alpha}{C_\alpha\ \Gamma(1+\alpha)}\,,\ \ (0 \le \alpha \le 1)\,, \tag{A.1}$$

where α is a number, $\Gamma(\cdot)$ is the Euler's Gamma Function, t $[s]$ is the time and C_α [Pa s^α] is a dimensional coefficient.

Clearly, when $\alpha = 0$, then $J(t) = \text{const}$: the response is linear elastic, with elastic modulus equal to C_0 [Pa] since $\Gamma(1) = 1$. When $\alpha = 1$, then $J(t)$ is a linear function of t, which corresponds to the classical Newton-Petroff viscous model with constant C_1 [Pa s] because $\Gamma(2) = 1$. In the general case, the coefficient α, with $0 \le \alpha \le 1$, continuously tunes the response from the pure elastic limit ($\alpha = 0$) to the pure viscous limit ($\alpha = 1$).

The Boltzmann superposition principle of linear viscoelasticity defines the strain history $\gamma(t)$ associated with a given stress history $\tau(t)$ as

$$\gamma(t) = \frac{1}{C_\alpha \Gamma(1+\alpha)} \int_0^t (t-\bar{t})^\alpha\, \dot{\tau}(\bar{t})\, d\bar{t}\,. \tag{A.2}$$

This expression is valid when the system is quiescent at $t = 0$, i.e., $\gamma(t) = 0$ and $\tau(t) = 0$ for $t \le 0$. Integration by parts provides the general constitutive law for the viscoelastic material in the form

$$\gamma(t) = \frac{1}{C_\alpha}\, {}_0\mathcal{I}_t^\alpha[\tau(\cdot)](t)\,, \tag{A.3}$$

where ${}_0\mathcal{I}_t^\alpha$ is the *Riemann-Liouville* (R-L) fractional integral of order α which, for any generic function $f(\cdot)$, is defined as

$${}_0\mathcal{I}_t^\alpha[f(\cdot)](t) = \frac{1}{\Gamma(\alpha)} \int_0^t (t-\bar{t})^{\alpha-1}\, f(\bar{t})\, d\bar{t}\,. \tag{A.4}$$

If one supposes that the strain history is assigned in the form $\gamma(t) = \mathcal{H}(t)$, the corresponding stress history will decay in time according to the *relaxation function* $R(t)$. Boltzmann superposition principle indicates that the stress history corresponding to an assigned strain history $\gamma(t)$ will be

$$\tau(t) = \int_0^t R(t-\bar{t})\dot{\gamma}(\bar{t})\, d\bar{t}\,. \tag{A.5}$$

The relaxation function $R(t)$ is related to the creep function $J(t)$ by the fundamental law of viscoelasticity

$$\widehat{J}(s)\,\widehat{R}(s) = s^{-2}\,, \tag{A.6}$$

where $\widehat{J}(s)$ and $\widehat{R}(s)$ are respectively the Laplace transforms of $J(t)$ and $R(t)$, having denoted with s the complex variable of the transformation. It can be demonstrated that if $J(t)$ is of the form (A.1), the corresponding $R(t)$ is given by

$$R(t) = \frac{C_\alpha}{\Gamma(1-\alpha)} t^{-\alpha}\,. \tag{A.7}$$

Using this expression in (A.5), one finds

$$\tau(t) = C_\alpha\, {}^{C}_{0}\mathcal{D}^{\alpha}_{t}[\gamma(\cdot)](t)\,, \tag{A.8}$$

where ${}^{C}_{0}\mathcal{D}^{\alpha}_{t}[\,\dots\,]$ is the Caputo's fractional derivative of order α, which is an operator transforming any function $f(\cdot)$ in

$${}^{C}_{0}\mathcal{D}^{\alpha}_{t}[f(\cdot)](t) = \frac{1}{\Gamma(1-\alpha)} \int_0^t (t-\bar{t})^{-\alpha}\, \dot{f}(\bar{t})\, d\bar{t}\,. \tag{A.9}$$

Also in this case, this expression is valid when $\gamma(t) = 0$ for $t \leq 0$. It can be directly verified through integration by parts, that if the system is at rest for $t \leq 0$, then the integral and differential operators commute, i.e.,

$${}_0\mathcal{I}^{\alpha}_{t}[{}^{C}_{0}\mathcal{D}^{\alpha}_{t}[\gamma(\cdot)]](t) = \gamma(t), \text{ or, formally, } {}_0\mathcal{I}^{\alpha}_{t}[\gamma(\cdot)](t) = {}^{C}_{0}\mathcal{D}^{-\alpha}_{t}[\gamma(\cdot)](t)\,. \tag{A.10}$$

In conclusion, equations (A.3) and (A.8) represent the constitutive laws of fractional viscoelasticity of order α. The operators are linear and, hence, the main properties of the classical derivatives and integral of integer order (linearity, semigroup properties) are still valid, even if integration by parts and Leibniz rule in general do

not hold true [58, 59]. In the Laplace domain, they exactly behave as the classical derivatives and integrals; for example

$$\mathcal{L}\left\{\frac{d^n f}{dt^n}, s\right\} = (s)^n \hat{f}(s)\,, \quad \mathcal{L}\left\{{}_0^C\mathcal{D}_t^\alpha[f], s\right\} = (s)^\alpha \widehat{f}(s)\,, \tag{A.11}$$

provided that the values of $f(t)$ and its derivatives up to $n-1$ are null at $t=0$.

It is often necessary to provide a numerical approximation of the fractional integral (A.4) and the fractional derivative (A.9). Assume to subdivide a time interval of interest $[0, T]$ in s subintervals whose amplitude is $\Delta t = t_j - t_{j-1}$. Then, take a generic continuous function denoted as $f(t)$, so that $f(t_j) = f_j$ and $\mathbf{f}_s^T = [f(t_1)\ f(t_2)\ \dots\ f(t_s)]$. The fractional integral and the fractional derivative of order α at the point t_j can be numerically approximated through Grünwald-Letnikov operators defined as

$${}_0\mathcal{I}_t^\alpha[f(\cdot)](t) \simeq (\nabla^{-\alpha} f)(t_j) = \Delta t^\alpha \sum_{r=0}^{j-1} \frac{\Gamma(r+\alpha)}{\Gamma(r+1)\Gamma(\alpha)} f(t_j - r\Delta t)\,, \tag{A.12}$$

$${}_0^C\mathcal{D}_t^\alpha[f(\cdot)](t) \simeq (\nabla^{\alpha} f)(t_j) = \Delta t^{-\alpha} \sum_{r=0}^{j-1} \frac{\Gamma(r-\alpha)}{\Gamma(r+1)\Gamma(-\alpha)} f(t_j - r\Delta t)\,. \tag{A.13}$$

These can be expressed in compact matrix form. The approximation of the fractional derivative is

$$\nabla^\alpha \mathbf{f}_s = \mathbf{A}_s^{(\alpha)} \mathbf{f}_s, \tag{A.14}$$

where $\mathbf{A}_s^{(\alpha)}$ is a $s \times s$ lower band strip matrix

$$\mathbf{A}_s^{(\alpha)} = \frac{1}{\Delta t^\alpha} \begin{bmatrix} \omega_1(\alpha) & & & \\ \omega_2(\alpha) & \omega_1(\alpha) & & \\ \vdots & \ddots & \ddots & \\ \omega_s(\alpha) & \dots & \omega_2(\alpha) & \omega_1(\alpha) \end{bmatrix}, \tag{A.15}$$

with $\omega_1 = 1$, $\omega_2 = -\alpha$, $\dots$, $\omega_{j+1} = \dfrac{j-\alpha-1}{j}\omega_j(\alpha)$. Obviously, by setting $\mathbf{B}_s^{(\alpha)} =$

$\mathbf{A}_s^{(-\alpha)}$, the matrix form of the fractional integral reads

$$\nabla^{-\alpha}\mathbf{f}_s = \mathbf{B}_s^{(\alpha)}\mathbf{f}_s. \tag{A.16}$$

Using this discretization, an intergral/differential fractional equation can be directly solved step-by-step. Of course the time step Δt has to be accurately chosen according to the input datum.

References

[1] P. Hooper, R. Sukhram, B. Blackman, and J. Dear, "On the blast resistance of laminated glass," *International Journal of Solids and Structures*, vol. 49, no. 6, pp. 899–918, 2012.

[2] J. Pelfrene, J. Kuntsche, S. V. Dam, W. V. Paepegem, and J. Schneider, "Critical assessment of the post-breakage performance of blast loaded laminated glazing: experiments and simulations," *International Journal of Impact Engineering*, vol. 88, pp. 61–71, 2016.

[3] L. Galuppi and G. Royer-Carfagni, "A homogenized analysis à la Hashin for cracked laminates under equi-biaxial stress. Applications to laminated glass," *Composites Part B: Engineering*, vol. 111, pp. 332–347, 2017.

[4] S. J. Bennison, A. Jagota, and C. A. Smith, "Fracture of glass/poly (vinyl butyral)(Butacite®) laminates in biaxial flexure," *Journal of the American Ceramic Society*, vol. 82, no. 7, pp. 1761–1770, 1999.

[5] A. V. Duser, A. Jagota, and S. J. Bennison, "Analysis of glass/polyvinyl butyral laminates subjected to uniform pressure," *Journal of engineering mechanics*, vol. 125, no. 4, pp. 435–442, 1999.

[6] A. Zemanová, J. Zeman, and M. Šejnoha, "Comparison of viscoelastic finite element models for laminated glass beams," *International Journal of Mechanical Sciences*, vol. 131, pp. 380–395, 2017.

[7] P. G. Nutting, "A new general law of deformation," *Journal of the Franklin Institute*, vol. 191, no. 5, pp. 679–685, 1921.

[8] G. W. S. Blair and J. E. Caffyn, "Vi. an application of the theory of quasi-properties to the treatment of anomalous strain-stress relations," *The London, Edinburgh, and Dublin Philosophical Magazine and Journal of Science*, vol. 40, no. 300, pp. 80–94, 1949.

[9] A. Gemant, "A method of analyzing experimental results obtained from elasto-viscous bodies," *Journal of Applied Physics*, vol. 7, no. 8, pp. 311–317, 1936.

[10] H. Schiessel and A. Blumen, "Hierarchical analogues to fractional relaxation equations," *Journal of Physics A: Mathematical and General*, vol. 26, no. 19, p. 5057, 1993.

[11] H. Schiessel, R. Metzler, A. Blumen, and T. F. Nonnenmacher, "Generalized viscoelastic models: their fractional equations with solutions," *Journal of physics A: Mathematical and General*, vol. 28, no. 23, p. 6567, 1995.

[12] N. Makris, "Three-dimensional constitutive viscoelastic laws with fractional order time derivatives," *Journal of Rheology*, vol. 41, no. 5, pp. 1007–1020, 1997.

[13] R. L. Bagley and P. J. Torvik, "Fractional calculus-a different approach to the analysis of viscoelastically damped structures," *AIAA journal*, vol. 21, no. 5, pp. 741–748, 1983.

[14] P. J. Torvik and R. L. Bagley, "On the appearance of the fractional derivative in the behavior of real materials," *Journal of Applied Mechanics, Transactions ASME*, vol. 51, no. 2, pp. 294–298, 1984.

[15] R. Bagley, "On the fractional calculus model of viscoelastic behavior," *Journal of Rheology*, vol. 30, no. 1, pp. 133–155, 1986.

[16] P. D. Spanos and G. I. Evangelatos, "Response of a non-linear system with restoring forces governed by fractional derivatives—time domain simulation and statistical linearization solution," *Soil Dynamics and Earthquake Engineering*, vol. 30, no. 9, pp. 811–821, 2010.

[17] A. Pirrotta, S. Cutrona, and S. Di Lorenzo, "Fractional visco-elastic Timoshenko beam from elastic Euler-Bernoulli beam," *Acta Mechanica*, vol. 226, no. 1, pp. 179–189, 2015.

[18] A. Pirrotta, S. Cutrona, S. Di Lorenzo, and A. Di Matteo, "Fractional viscoelastic Timoshenko beam deflection via single equation," *International Journal for Numerical Methods in Engineering*, vol. 104, no. 9, pp. 869–886, 2015.

[19] M. Di Paola, R. Heuer, and A. Pirrotta, "Fractional visco-elastic Euler–Bernoulli beam," *International Journal of Solids and Structures*, vol. 50, no. 22-23, pp. 3505–3510, 2013.

[20] M. Di Paola, A. Pirrotta, and A. Valenza, "Visco-elastic behavior through fractional calculus: an easier method for best fitting experimental results," *Mechanics of materials*, vol. 43, no. 12, pp. 799–806, 2011.

[21] M. Di Paola, L. Galuppi, and G. Royer Carfagni, "Fractional viscoelastic characterization of laminated glass beams under time-varying loading," *International Journal of Mechanical Sciences*, vol. 196, p. 106274, 2021.

[22] P. S. Bulson, *Explosive loading of engineering structures*. CRC Press, 1997.

[23] G. F. Kinney and K. J. Graham, *Explosive shocks in air*. Springer Science & Business Media, 2013.

[24] EN 13123-1, *Windows, doors and shutters-explosion resistance - requirements and classification - Part 1: shock tube*. 2001-10.

[25] EN 13123-2, *Windows, doors and shutters-explosion resistance - requirements and classification - Part 2: range test*. 2004-05.

[26] EN 13124-1, *Windows, doors and shutters-explosion resistance - test method - Part 1: shock tube*. 2001-10.

[27] EN 13124-2, *Windows, doors and shutters-explosion resistance - test method - Part 1: range test*. 2004-05.

[28] GSA (General Services Administration), "Standard test method for glazing and window systems subject to dynamic overpressure loadings," 2003.

[29] L. Galuppi and G. Royer-Carfagni, "Laminated beams with viscoelastic interlayer," *International Journal of Solids and Structures*, vol. 49, no. 18, pp. 2637–2645, 2012.

[30] L. Galuppi and G. Royer-Carfagni, "The design of laminated glass under time-dependent loading," *International Journal of Mechanical Sciences*, vol. 68, pp. 67–75, 2013.

[31] J. Eisenträger, K. Naumenko, H. Altenbach, and H. Köppe, "Application of the first-order shear deformation theory to the analysis of laminated glasses and photovoltaic panels," *International Journal of Mechanical Sciences*, vol. 96, pp. 163–171, 2015.

[32] M. Amabili, P. Balasubramanian, R. Garziera, and G. Royer-Carfagni, "Blast loads and nonlinear vibrations of laminated glass plates in an enhanced shear deformation theory," *Composite Structures*, vol. 252, p. 112720, 2020.

[33] L. Bardella, L. Paterlini, and A. Leronni, "Accurate modelling of the linear elastic flexure of composite beams warped by midlayer slip, with emphasis on concrete-timber systems," *International Journal of Mechanical Sciences*, vol. 87, pp. 268–280, 2014.

[34] A. Kumar, A. Chakrabarti, and P. Bhargava, "Finite element analysis of laminated composite and sandwich shells using higher order zigzag theory," *Composite Structures*, vol. 106, pp. 270–281, 2013.

[35] A. Kumar, A. Chakrabarti, and P. Bhargava, "Accurate dynamic response of laminated composites and sandwich shells using higher order zigzag theory," *Thin-Walled Structures*, vol. 77, pp. 174–186, 2014.

[36] A. Kumar, A. Chakrabarti, P. Bhargava, and V. Prakash, "Efficient failure analysis of laminated composites and sandwich cylindrical shells based on higher-order zigzag theory," *Journal of Aerospace Engineering*, vol. 28, no. 4, 2015.

[37] A. Kumar, A. Chakrabarti, P. Bhargava, and R. Chowdhury, "Probabilistic failure analysis of laminated sandwich shells based on higher order zigzag theory," *Journal of Sandwich Structures & Materials*, vol. 17, no. 5, pp. 546–561, 2015.

[38] A. Kumar, "Ultimate strength analysis of laminated composite sandwich plates," in *Structures*, vol. 14, pp. 95–110, Elsevier, 2018.

[39] M. Abualnour, A. Chikh, H. Hebali, A. Kaci, A. Tounsi, A. A. Bousahla, and A. Tounsi, "Thermomechanical analysis of antisymmetric laminated reinforced composite plates using a new four variable trigonometric refined plate theory," *Computers and Concrete*, vol. 24, no. 6, pp. 489–498, 2019.

[40] M. Sahla, H. Saidi, K. Draiche, A. A. Bousahla, F. Bourada, and A. Tounsi, "Free vibration analysis of angle-ply laminated composite and soft core sandwich plates," *Steel and Composite Structures*, vol. 33, no. 5, pp. 663–679, 2019.

[41] K. Draiche, A. A. Bousahla, A. Tounsi, A. S. Alwabli, A. Tounsi, and S. R. Mahmoud, "Static analysis of laminated reinforced composite plates using a simple first-order shear deformation theory," *Computers and Concrete*, vol. 24, no. 4, pp. 369–378, 2019.

[42] N. Belbachir, K. Draich, A. A. Bousahla, M. Bourada, A. Tounsi, and M. Mohammadimehr, "Bending analysis of anti-symmetric cross-ply laminated plates under nonlinear thermal and mechanical loadings," *Steel and Composite Structures*, vol. 33, no. 1, pp. 81–92, 2019.

[43] N. Belbachir, M. Bourada, K. Draiche, A. Tounsi, F. Bourada, A. A. Bousahla, and S. R. Mahmoud, "Thermal flexural analysis of anti-symmetric cross-ply laminated plates using a four variable refined theory," *Smart Structures and Systems*, vol. 25, no. 4, pp. 409–422, 2020.

[44] O. Allam, K. Draiche, A. A. Bousahla, F. Bourada, A. Tounsi, K. H. Benrahou, S. R. Mahmoud, E. A. A. Bedia, and A. Tounsi, "A generalized 4-unknown refined theory for bending and free vibration analysis of laminated composite and sandwich plates and shells," *Computers and Concrete, An International Journal*, vol. 26, no. 2, pp. 185–201, 2020.

[45] J. A. Hooper, "On the bending of architectural laminated glass," *International Journal of Mechanical Sciences*, vol. 15, no. 4, pp. 309–323, 1973.

[46] L. Galuppi and G. Royer-Carfagni, "Effective thickness of laminated glass beams: New expression via a variational approach," *Engineering Structures*, vol. 38, pp. 53–67, 2012.

[47] J. Schlaich and T. Schober, H.and Moschner, "Prestressed cable-net façades," *Structural engineering international*, vol. 15, no. 1, pp. 36–36, 2005.

[48] W. Sobek, S. Feierabend, L. Blandini, and F. Tarazi, "Cable-stayed glass façades-15 years of innovation at the cutting edge," in *Challenging Glass Conference Proceedings*, vol. 2, pp. 599–608, 2010.

[49] G. Royer-Carfagni and L. Viviani, "Basic design of cable-supported glazed surfaces under blast waves," *International Journal of Non-Linear Mechanics*, vol. 123, p. 103489, 2020.

[50] International Organization for Standardization (ISO 16933:2007), "Glass in building—explosion-resistant security glazing—test and classification for arena air-blast loading," 2007.

[51] M. D. Goel, V. A. Matsagar, A. K. Gupta, and S. Marburg, "An abridged review of blast wave parameters," *Defence Science Journal*, vol. 62, no. 5, pp. 300–306, 2012.

[52] C. N. Kingery and G. Bulmash, "Technical report ARBRL-TR-02555: air blast parameters from TNT spherical air burst and hemispherical burst," *AD-B082*, vol. 713, 1984.

[53] X. Centelles, F. Pelayo, M. J. Lamela-Rey, A. I. Fernández, R. Salgado-Pizarro, J. R. Castro, and L. F. Cabeza, "Viscoelastic characterization of seven laminated glass interlayer materials from static tests," *Construction and Building Materials*, vol. 279, p. 122503, 2021.

[54] M. L. Williams, R. F. Landel, and J. D. Ferry, "The temperature dependence of relaxation mechanisms in amorphous polymers and other glass-forming liquids," *Journal of the American Chemical society*, vol. 77, no. 14, pp. 3701–3707, 1955.

[55] L. Biolzi, S. Cattaneo, M. Orlando, L. Ruggero Piscitelli, and P. Spinelli, "Constitutive relationships of different interlayer materials for laminated glass," *Composite Structures*, vol. 244, p. 112221, 2020.

[56] X. Chen, S. Chen, , and G.-Q. Li, "Experimental investigation on the blast resistance of framed pvb-laminated glass," *International Journal of Impact Engineering*, vol. 149, p. 103788, 2021.

[57] J. Wei and L. R. Dharani, "Response of laminated architectural glazing subjected to blast loading," *International Journal of Impact Engineering*, vol. 32, no. 12, pp. 2032–2047, 2006.

[58] V. E. Tarasov, "No violation of the leibniz rule. no fractional derivative," *Communications in Nonlinear Science and Numerical Simulation*, vol. 18, no. 11, pp. 2945–2948, 2013.

[59] V. E. Tarasov, "Leibniz rule and fractional derivatives of power functions," *Journal of Computational and Nonlinear Dynamics*, vol. 11, no. 3, p. art. n. 031014, 2016.